ACS OMEGA

Article

Cite This: ACS Omega 2018, 3, 7567−7579

Image-Guided Development of Heterocyclic Sulfoxides as Ligands for Tau Neurofibrillary Tangles: From First-in-Man to Second-Generation Ligands

Waqas Rafique,[†] Vasko Kramer,[#,∇] Tania Pardo,[∥] René Smits,[⊥] Mona M. Spilhaug,[†] Alexander Hoepping,[⊥] Eduardo Savio,[∥] Henry Engler,[∥] Rodrigo Kuljs,[○] Horacio Amaral,[#,∇] and Patrick J. Riss*[,†,‡,§]

[†]Realomics SRI, Kjemisk Institutt, Universitetet i Oslo, Sem Sælands vei 26, Kjemibygningen, 0371 Oslo, Norway

[‡]Klinik for Kirurgi og Nevrofag, Oslo Universitets Sykehus HF—Rikshospitalet, Postboks 4950 Nydalen, 0424 Oslo, Norway

[§]Norsk Medisinsk Syklotronsenter AS, Gaustad, Postboks 4950 Nydalen, 0424 Oslo, Norway

[∥]Departamento de Montevideo, Uruguayan Centre of Molecular Imaging (CUDIM), Av. Dr. Américo Ricaldoni 2010, 11600 Montevideo, Uruguay

[⊥]Advanced Biochemical Compounds GmbH, Heinrich-Glaeser-Strasse 10-14, D-01454 Radeberg, Germany

[#]Positronpharma SA, Rancagua 878, 7500921 Providencia, Santiago, Chile

[∇]Center of Nuclear Medicine Positronmed, Julio Prado 714, 7501068 Providencia, Santiago, Chile

[○]Zdrav Mozak Clinical Neuroscience Center, Julio Prado 714, 7501068 Providencia, Santiago, Chile

Supporting Information

ABSTRACT: Positron emission tomography (PET) imaging of misfolded protein aggregates that form in neurodegenerative processes of the brain is key to providing a robust marker for improved diagnosis and evaluation of treatments. We report the development of advanced radiotracer candidates based on the sulfoxide scaffold found in proton pump inhibitors (lansoprazole, prevacid) with inherent affinity to neurofibrillary tangles in Alzheimer's disease and related disorders (e.g., dementia with Lewy bodies and the frontotemporal degeneration syndrome). First-in-man results obtained with [^{18}F]lansoprazole and *N*-methyl-[^{18}F]lansoprazole were used to guide the design of a set of 24 novel molecules with suitable properties for neuroimaging with PET. Compounds were synthesized and characterized pharmacologically, and the binding affinity of the compounds to synthetic human tau-441 fibrils was determined. Selectivity of binding was assessed using α-synuclein and β-amyloid fibrils to address the key misfolded proteins of relevance in dementia. To complete the pharmacokinetic profiling in vitro, plasma protein binding and lipophilicity were investigated. Highly potent and selective new radiotracer candidates were identified for further study.

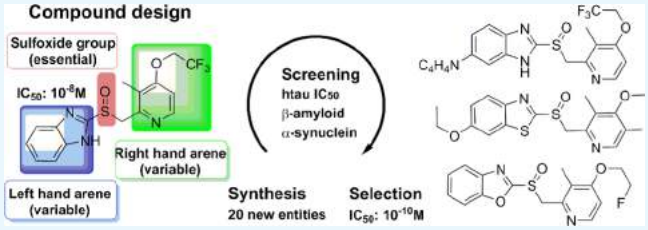

INTRODUCTION

Alzheimer's disease (AD) is a progressive neurodegenerative disease of ageing, characterized by a gradual decline of cognitive and behavioral performances and subsequent deterioration of activities in daily living. Because the diagnosis based solely on clinical manifestations is imprecise and may thus lead to difficulties, means to accurately diagnose the underlying molecular pathology, as well as to monitor the effects of strategies for therapeutic intervention, are required to mitigate the escalating impact of the disease worldwide.[1−4] Abnormal aggregation of a microtubular protein called tubule-associated unit (tau) is widely felt to be implicated in neurodegenerative diseases, such as AD, frontotemporal degeneration, progressive supranuclear palsy, corticobasal degeneration, and chronic traumatic encephalopathy.[5−8] Misfolded fragments of tau form aggregates of fibrillar matter named neurofibrillary tangles (NFTs) inside neurons when a threshold concentration is exceeded. Although monomers are believed to cause damage, the presence of NFTs is a definitive endpoint of progressing disease and can be imaged using positron emission tomography (PET) for diagnosis, treatment development, and evaluation.[9−12]

Despite the promising results in clinical studies using investigational radioligands for tau imaging, the first generation of radiotracers designed for the detection of NFTs in brain is not yet suitable for routine clinical use. Low specific signal in brain, heterogeneous nonspecific binding, blood−brain barrier penetrating radiometabolites, and cross-affinity to other

Received: May 11, 2018
Accepted: June 15, 2018
Published: July 9, 2018

DOI: 10.1021/acsomega.8b00975
ACS Omega 2018, 3, 7567−7579

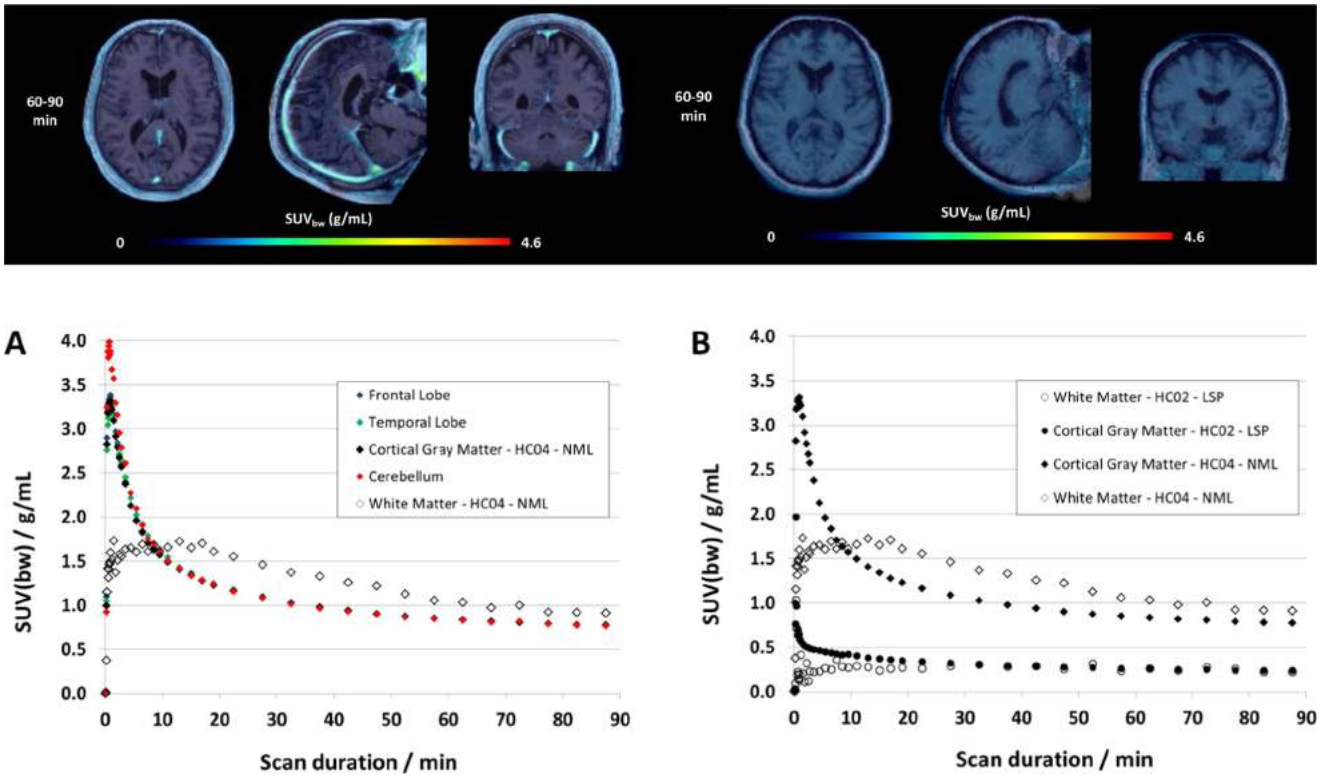

Figure 1. Top: transversal, sagittal, and coronal views of averaged PET/MRI fusion images of [^{18}F]**1** (left) and [^{18}F]**2** (right) 75 min postinjection. Bottom: (A) time−activity curves (TACs) of [^{18}F]**2** in the frontal lobe (blue), temporal lobe (green), cortical gray matter (black), white matter (white), and cerebellum (red); (B) comparison of TACs for [^{18}F]**1** (circles) and [^{18}F]**2** (diamonds) in cortical gray and white matter, respectively.

proteins hamper the current application of the technology.[13−15] For instance, [^{18}F]T807 has shown to bind to monoamino oxidase A with high affinity, which might contribute to tracer binding in tau-rich regions outside the striatum.[15] [^{18}F]THK-5351, another tau tracer currently in clinical trials, shows high affinity for monoamino oxidase B, which is expressed in activated microglia, associated with inflammation and neurodegeneration and which also contributes to nonspecific binding in relevant brain regions. Therefore, further investigation is needed to obtain more specific radiotracers with an improved clinical scope for the detection of NFTs in the brain.

Our objective is to identify new, specific ligands binding to synthetic aggregated paired helical filaments (PHFs) of human tau (hTau).[16] In practice, only lipophilic small molecules (M < 450 g/mol) labeled with the short-lived radionuclides ^{11}C ($t_{1/2}$ = 20 min) or ^{18}F ($t_{1/2}$ = 110 min) provide optimal chemical, physical, and pharmacological properties for design of reversibly binding PET radiotracers. Because of the cost and handling constraints originating from a short half-life, clinical radiotracers should preferably be labeled with ^{18}F.

NFTs are challenging targets for small-molecule ligands. In contrast to functional proteins, they constitute macromolecular assemblies composed of misfolded tau fragments. These fragments are formed in low concentration during the progression of neurodegenerative diseases and do not possess functional binding pockets. Most known ligands are derived from aromatic dyes binding to residual β-sheet folds in the NFT superstructure, which complicates selective detection of NFTs over other misfolded proteins with intrinsic β-sheet structures, e.g., β-amyloid or α-synuclein.[17−21]

RESULTS AND DISCUSSION

Lead Validation in Clinical Imaging. Proton pump inhibitor lansoprazole (**1**, 2-(((3-methyl-4-(2,2,2-trifluoroethoxy)pyridin-2-yl)methyl)sulfinyl)-1*H*-benzoimidazole) caught our attention when NFT binding and some inherent selectivity over other misfolded protein aggregates were associated with the drug.[22−25] For lead compounds astemizole and lansoprazole, in vitro affinities of 1.9 ± 0.1 and 2.5 ± 0.4 nM to heparin-induced tau filaments (HITFs) and 2.1 ± 0.1 and 830 ± 180 nM to paired helical tau filaments (PHF-Tau) were determined by radioligand binding assays.[22] The selective interaction of **1** with PHF-Tau was further proved by a comparison of immunohistochemical staining of PHF-Tau. Although it was not possible to obtain crystal structures of the native tau protein to obtain information about the binding site of **1**, the authors were able to show a strong interaction of **1** with hexapeptide 386TDHGAE391 located in the center of PHF-Tau. Taking these promising preclinical results into account, **1** as a registered medicinal product is safe and well suited for human application, which allowed for PET studies to deduce the risk of progressing with the compound. Hence, we initiated a first-in-man PET study in a small group of healthy volunteers to obtain information on the kinetic profile of ^{18}F-labeled lansoprazole in the brain. To our dismay, [^{18}F]**1** had a very limited brain uptake because of N−H-acidity (pK_a ∼ 4) of the imidazolyl sulfoxide moiety.[25] Another hypothetical culprit may be near quantitative plasma protein binding; the irreversible, covalent mechanism of action as a proton pump inhibitor; or active transport via multidrug resistance-proteins.[25]

Previous experiments in animals suggested that methylation of the nitrogen in the benzimidazole scaffold leads to higher

DOI: 10.1021/acsomega.8b00975
ACS Omega 2018, 3, 7567−7579

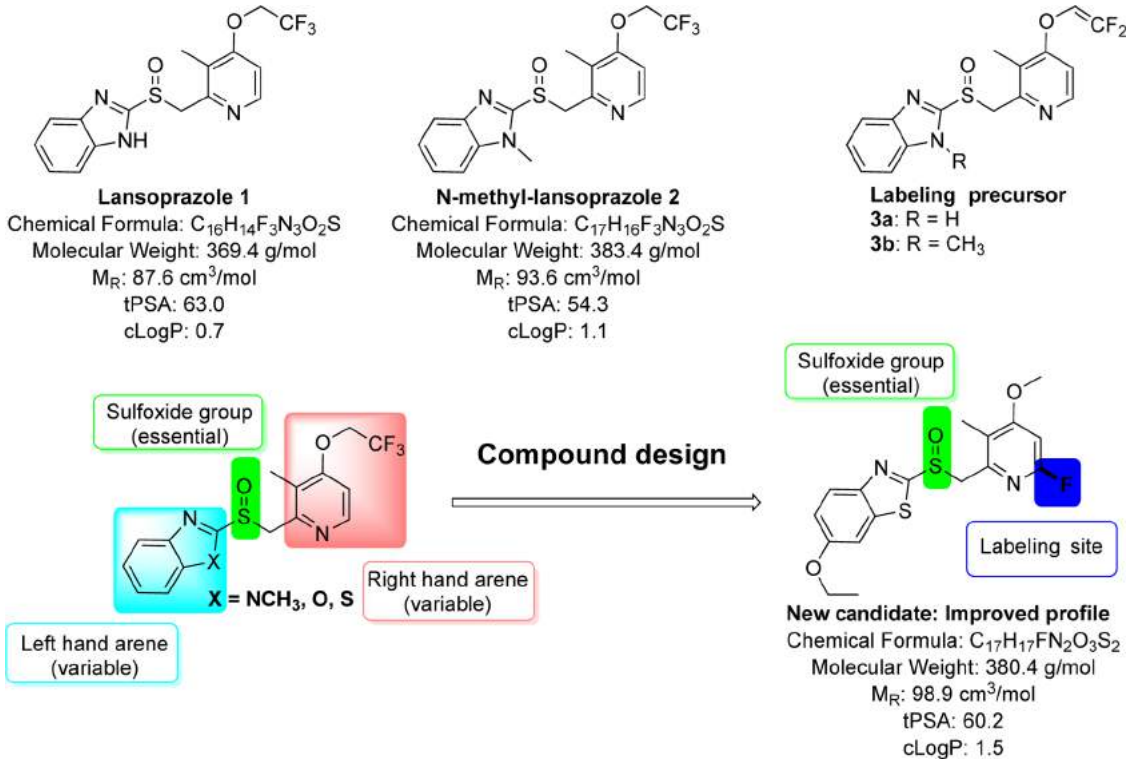

Figure 2. Top: lansoprazole (**1**) and *N*-methyl-lansoprazole (**2**) the original leads. Bottom: dissection of lansoprazole into building blocks (blue, green) and generic scheme depicting the design of new analogues.

brain uptake; however, clinical data has not been reported to the best of our knowledge. We therefore progressed with a clinical study to investigate *N*-methyl-[^{18}F]lansoprazole ([^{18}F]**2**) in comparison to lead [^{18}F]**1**. The study was approved by the regional Ethics Committee (SSM Oriente), and written informed consent was obtained from all subjects. Inclusion criteria for all participants were age of 50−70 years, not having clinical signs of any neurological or psychiatric disorder, and using anticontraceptives for at least 6 months after last imaging visit in case of possible pregnancy. [^{18}F]**1** was obtained in 1.4 ± 0.5% radiochemical yield (RCY) with >98% radiochemical purity (RCP) and molar activity (A_m) of 80−98 GBq/μmol (2.5 Ci/μmol). [^{18}F]**2** was obtained in 2.1 ± 1.4% RCY with >98% RCP and molar activity of 230−310 GBq/μmol (6 Ci/μmol). A total of four healthy volunteers (mean age 60.2 ± 6.0 years) were included to study the physiological distribution of [^{18}F]**1** and [^{18}F]**2** in the human brain. All subjects received a single intravenous bolus injection of 300−350 MBq of either [^{18}F]**1** or [^{18}F]**2** with an injected mass in the range of 0.1−1.5 μg. PET images were corrected for motion, fused to individual T1-weighted magnetic resonance imaging (MRI) or computed tomography scans, and normalized to Montreal Neurological Institute (MNI) space. Standard volume of interest (VOI) maps were outlined from the available brain atlas in MNI space for frontal cortex, temporal cortex, parietal cortex, occipital cortex, whole brain, white matter, and cerebellar cortex as reference regions. Time−activity curves (TACs) were calculated for all brain regions, and brain uptake was calculated in percent injected dose (% i.D.) in the whole brain at different time points.

For the whole brain, peak uptakes of 2.5−3.5% i.D. for [^{18}F]**1** and 5.0−6.0% i.D. for [^{18}F]**2** were observed during the initial perfusion phase 1 min postinjection (p.i.). For [^{18}F]**1**, most of the activity was confined to the venous vascularization, dropping fast to less than 1.0% i.D. at 2 min p.i. and below 0.5% after 90 min. [^{18}F]**2** showed good penetration into brain tissue and fast, homogeneous clearance from the brain. Radioactivity concentrations in brain were about 3.0, 2.0, and 1.3% of the injected dose at 10, 27, and 90 min, respectively. In general, an uptake of 3.0−5.0% i.D. in brain can be considered suitable for the application of a tracer for neuroimaging. The comparative study revealed attractive characteristics for radiotracer development inherent to the scaffold. Fast clearance and no indications on binding to targets in the healthy brain other than in white matter have been observed (Figure 1).

Of particular importance here is the complete absence of specific binding in any brain region including the striatum, indicating that lead [^{18}F]**2** has a negligible affinity toward monoamino oxidase A and B, typically expressed in this region. The phenomenon of white matter binding is in accordance with previously reported results observed for other NFT PET tracers, perhaps related to the high amount of β-sheet-rich myelin tissue in white matter. This is not a desired characteristic for a tau imaging agent but confirms the brain penetration of the tracer and is not an issue for further progression as it is cleared rapidly from the tissue.

On this basis, we decided to develop the lead into a library of new ligands with a chemical and pharmacological profile suitable for PET imaging, in particular by increasing the in vitro affinity toward HITF and the selectivity over α-synuclein and β-amyloid fibrils and by increasing brain permeability.

Compound Design. The scaffold of **1** was used as a template to design molecules with the desired physical, chemical, and pharmacological characteristics. During the design phase, permeative properties derived from in silico

DOI: 10.1021/acsomega.8b00975
ACS Omega 2018, 3, 7567−7579

Scheme 1. Illustration of the Synthesis Routes to Pyridines 8a−f

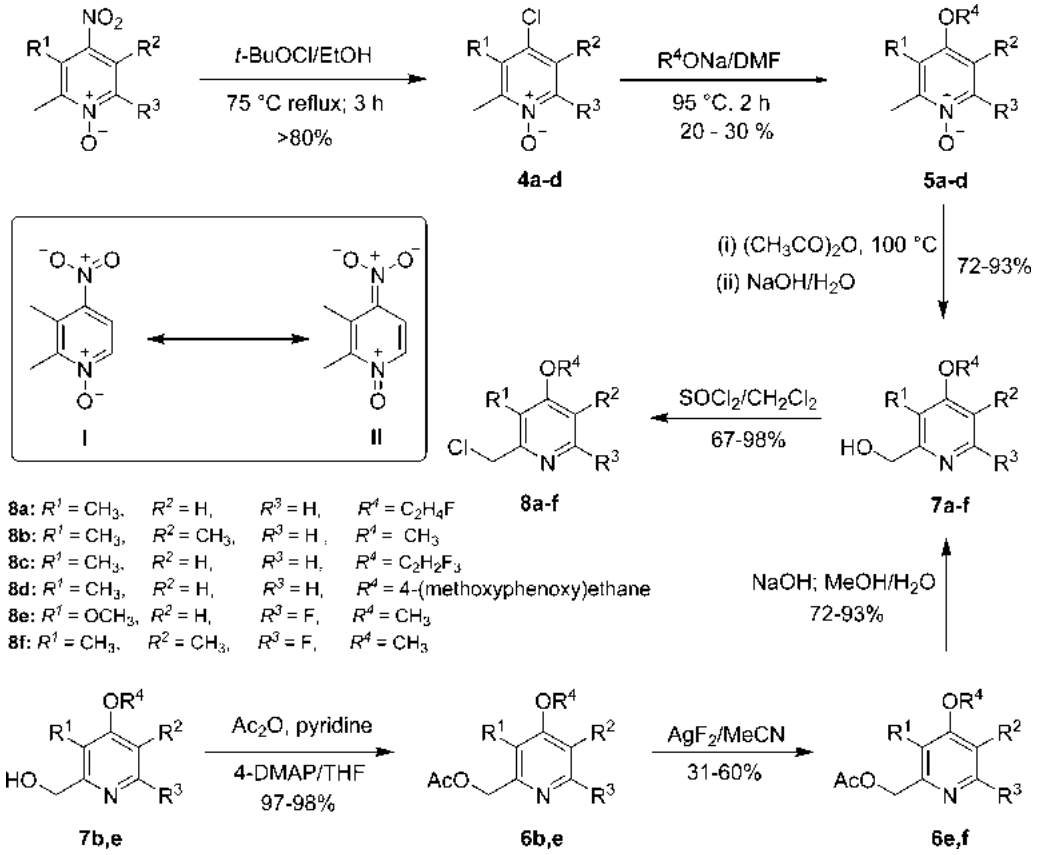

data such as polar surface area (tPSA), partition coefficients (log *P*, log $D_{7.4}$), molecular weight, and molecular volume were used for guidance.[26,27] Figure 2 shows the lead radioligands and the design of new derivatives.

Using retrosynthesis, the lead was segmented into three building blocks: the heteroaryl building block (variable, blue), the central sulfoxide function (green), and the arylmethyl building block (variable, red). New compounds were designed by combining such basic building blocks in silico. The library obtained was filtered for key criteria of relevance for its purpose. For example, the combined mass of all three components should not exceed 450 g/mol and one moiety should allow for direct, nucleophilic radiolabeling using no-carrier-added [^{11}C]CH_3I and/or ^{18}F-fluoride ion. Particular emphasis was put on mapping the activity and selectivity of new derivatives devoid of the benzimidazol-N−H function. The following selection criteria were applied (in weighted order):

1. Polar surface area <80 Å^2
2. Aliphatic, primary C−F bond
3. Log $D_{7.4}$ > log *P*; 1.5
4. Molecular weight, *M* < 450 g/mol
5. Molecular volume, V_m (candidate) = V_m(lead) ± 15%
6. Aliphatic, secondary C−F bond or aromatic C−F bond

Synthesis of Compounds. To obtain new derivatives based on these constraints, building blocks were synthesized when necessary or procured when commercially available. Segmentation into such simple building blocks facilitated the synthesis of final compounds in only two synthetic steps. The compound library closely resembled the original template under exclusion of the acidic proton. A number of compounds accommodate reliable ^{18}F-labeling protocols and some structural variation.

Despite several attempts, the nitro-function in the starting material proved to be difficult to substitute for alkoxy substituents directly. In addition, some nucleophiles such as sodium *p*-methoxybenzylate and sodium *tert*-butyl-dimethylsilylate underwent oxidation even under Ar or N_2 as observed by NMR. We attributed the issue to an unusually stable isomer,[28] formed in an intramolecular attack centered on a hyperconjugated pyridine nitrogen to form (1-oxopyridin-1-ium-4(1*H*)-ylidene)azinate (Scheme 1, II). The intermediate would constitute a stable compound with low electrophilicity on the ipso-carbon of the leaving group, thus preventing the Meisenheimer complex necessary for S_NAr reactions. To circumvent the issue, we introduced a chloro substituent using *tert*-butyl hypochloride (*t*-BuOCl) to obtain the 4-chloropyridine analogues in 80−95% yield.[29−31] Substitution of the chloride was still hampered by somewhat low yields and competing formation of oxidation products. An optimization of the reaction conditions led to the omission of excess alcoholic solvent; instead, 3 equiv of 2-fluoroethanol was added dropwise to dimethylformamide containing stoichiometric NaH. The obtained solution was reacted with **4a−d** to afford alkyl aryl ether **5a−d** in only 25% yield.[42] Ether **5a−d** was converted to pyridine derivative **7a−d** using a sequence of transformations. In brief, acylation of the N-oxide, followed by a [3,3]-sigmatropic rearrangement was used to install the benzylic oxy-function. Hydrolysis of the acetyl intermediate with NaOH afforded the product in 72−93% yield over three steps in one pot. Compound **7a−f** was treated with thionyl chloride to obtain the pyridine building block **8a−f** in 67−98%

DOI: 10.1021/acsomega.8b00975
ACS Omega 2018, 3, 7567−7579

Scheme 2. General Scheme for the Synthesis of Final Compounds over Two Steps

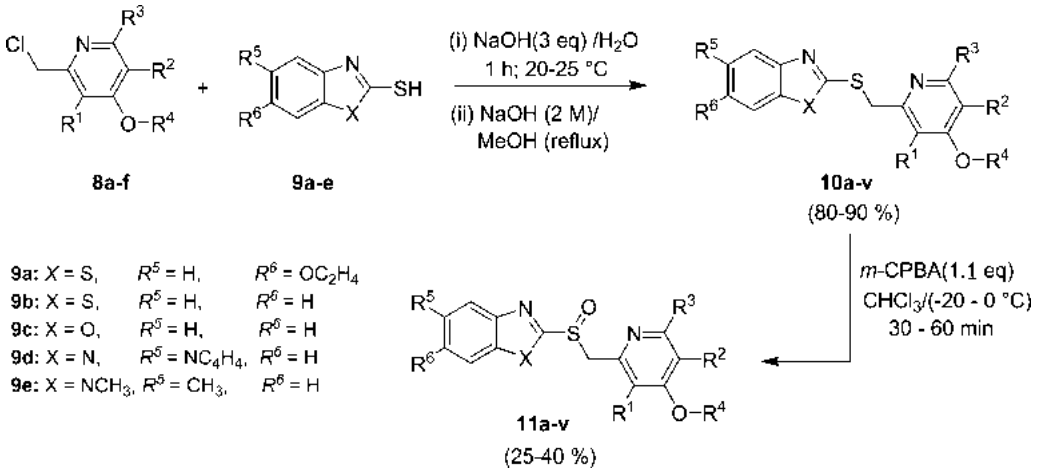

yield.[32,33] Via this route, pyridines were synthesized in an overall yield of about 10% over six steps.

Pyridine fluorination was achieved on intermediates **6b** and **6e** using the method of Fier and Hartwig.[34] Because of technical limitations, AgF_2 had to be handled without the precautions indicated by the authors. As a result, best yields were obtained when using fresh AgF_2. Nonetheless, we obtained a 60% yield with fresh AgF_2 in contrast to the original report of 81% isolated fluoropyridine **6e**. An aged sample of silver difluoride in stock gave only 31% **6f**.

Final compounds were obtained under fairly mild conditions as follows. Compounds **9a−e** were treated with aqueous NaOH (3 equiv) and allowed to react with pyridines **8a−f** for 1 h at room temperature (rt). Compounds **10a−v** were isolated in an overall yield of 70−90% and characterized. Isolation is not strictly necessary prior to the final oxidation, which eased scale-up of the reaction. Direct oxidation to furnish radiotracer candidates **11a−v** was achieved with *meta*-chloroperbenzoic acid (*m*-CPBA, 1.1 equiv) in low to moderate yields of 25−40%. We attributed some low yield to overoxidation of the sulfur and nitrogen. However, no further attempts were made to optimize the reaction at this point because sufficient amounts were available for biological studies (Scheme 2).

Characterization. Traditionally, binding of candidate molecules to the target of interest is the first and foremost selection criterion for the development of a PET radiotracer. To visualize a target, a reasonable ratio between the available number of binding sites (B_{avail}) and dissociation constant k_d, also termed binding potential, is crucial. In the case of misfolded protein pathology, the expression patterns differ between diseases, from subject to subject and with the disease stage.[2−4,35] Therefore, we surmised that an optimal candidate would (1) bind to hTau-441 NFT with equal or better affinity than lead compounds **1** and **2** and (2) have a suitable selectivity for NFT over α-synuclein and β-amyloid and show better brain uptake. We tested all compounds for their binding characteristics to hTau-441, α-synuclein, and β-amyloid fibrils. A number of reference compounds were included to improve our understanding of the structure−activity relationship between imidazolyl-sulfoxides and misfolded protein aggregates. In addition to binding, we had to keep in mind the insufficient brain uptake of the lead structure, which leads us to investigate additional pharmacological parameters such as the lipophilicity and the protein-bound fraction in plasma of each candidate.

Because the purity of each test compound had to be determined prior to binding studies, we devised a purpose-made high-performance liquid chromatography (HPLC) method derived from OECD guidelines for testing of chemicals.[36] The HPLC method was calibrated using 30 reference compounds to allow for simultaneous determination of purity and of the distribution coefficient $\log D_{7.4}$ as a surrogate of lipophilicity (Supporting Information).

To assess the effect of structural modification on plasma protein binding, a plasma dialysis method was developed and validated. Porcine full blood was used because of its similarity to human blood. Samples were obtained, and plasma was separated. Following incubation of compounds **11a−v** as well as internal standards, plasma was subjected to membrane dialysis and the protein-free plasma samples were analyzed by HPLC (Supporting Information). Plasma protein binding remained high for all compounds in both pig and human blood. Notable exceptions include compounds **11e** and **11o,** which show a remarkable drop in activity of 10−20% relative to the rest of the series.

To determine the interaction of the new compounds with different misfolded proteins, we compared their in vitro binding affinity toward synthetic fibrils composed of hTau-441, α-synuclein, and β-amyloid. We decided to work with synthetic fibrils in this stage to avoid issues commonly associated with screening for binding in tissue samples. The main disadvantage of binding assays performed with the human (or animal) tissue specimen is false positive assessment of the binding profile, particularly when working with misfolded protein pathology. This is due to low target expression on one hand and substantial co-localization of functional proteins (e.g., butyryl choline esterase and monoamino oxidase) in both tau and amyloid brain lesions on the other. Reversible binding to these proteins may have mislead researchers in their structural optimization efforts, thus creating a cross-affinity to additional targets as reported previously. Nevertheless, we intend to evaluate the most promising candidates identified in this work by autoradiography (AR) on human tissue at a later time points to verify their affinity toward PHF-Tau.

Binding Affinity to hTau-441. Synthetic fibrils were prepared by aggregation of hTau-441 in the presence of Heparin at 37 °C for 7 days during which the aggregation

DOI: 10.1021/acsomega.8b00975
ACS Omega 2018, 3, 7567−7579

process was monitored by light scattering to investigate the size of the aggregate fibrils. At baseline conditions, only one distinct species with a hydrodynamic radius, r_h, of 322 nm was detected. At later time points up to 7 days, this species pertained (r_h = 322 nm) alongside some larger aggregates and small fragments. A globular protein of 60 kDa mass has an approximate r_h of 3.4 nm, which increases to about 5.1 nm at 150 kDa, which suggests that distinct aggregates are already present after 1 day of incubation.

In addition, we validated the fibrils and assay conditions for every aggregation batch by verifying maximum binding, displacement, and dissociation constant (k_d) using [^{3}H]-astemizole as the reference ligand as previously described.[22] Therefore, synthetic fibrils were freshly suspended in buffer and incubated with the radioligand in the presence of increasing concentration of 1×10^{-10}−3×10^{-5} M non-radioactive astemizole and the calculated k_d was compared to literature values for quality control.

Binding affinities of new reference compounds toward hTau-441 fibrils were determined by inhibition of [^{3}H]astemizole measured by autoradiography (AR) and at radioligand concentrations that gave the best specific signal. Reference compounds were tested at 10 concentrations spanning 1×10^{-10}−1×10^{-5} M, and inhibition potency was determined (half-maximal inhibitory concentration (IC_{50})).

Of a total of 24 newly synthesized compounds, we obtained reliable data for 19 compounds in the range of 0.2−100.0 nM (IC_{50}). Derivatives containing the ethoxy-substituted (**11a**, **11d**, and **11g**) and nonsubstituted "azol" structures are almost devoid of any simple trend of potency. It appears that fluorine or fluorinated aliphatic moieties are tolerated to a lesser extent, perhaps reflecting electrostatic or steric effects in the binding environment. As a result, the presence of the 4-methoxypyridine residue is highly beneficial for the overall potency (**11d**−**f**). Again, some trend is observed within the respective benzothiazole series throughout all pyridine moieties (e.g., **11a**, **11d**, and **11g**), of which the more electron-rich methoxy derivative (**11d**) demonstrates the highest potency of this series.

In contrast, introduction of the electron-withdrawing pyrrole substituent affects binding in a different way and the lowest affinity is found for the of the *N*-methyl imidazoles series (**11k**, **11n**, and **11q**). In fact, the rotamers show a remarkable distinction of their respective potencies (see Supporting Information for structure assignment by NMR). Whereas the corresponding syn-series (**11l**, **11o**, and **11r**) shows low nanomolar inhibition potency, the syn-analogues are between 8- and 20-fold less affine and require such high ligand concentration for displacement of astemizole that we approached the edge of quantification in our assay. Another intriguing observation is the pronounced effect of the imidazole-N−H function within the pyrrole series (**11j** and **11p**). Relative to the other pyrrolyl derivatives, these two molecules are remarkably potent binders of hTau but show only a small increase in inhibition binding to α-synuclein and β-amyloid. These findings indicate that the imidazole proton or its direct vicinity plays a major role in both the binding affinity and selectivity of binding among the three misfolded protein species. Unfortunately, pronounced N−H-acidity in these derivatives renders brain uptake very unlikely.

Interestingly, *N*-methyl derivatives devoid of the pyrrole substituent did not show significant affinity toward hTau-441, except compound **11t**, which binds with very high affinity. Phenomenologically, this may be attributed to the lack of conformational rigidity because no stable rotamers are present in these structures.

Nonetheless, in the light of these results, we plan to carry forward **11d**, **11i**, **11j**, and **11t** for direct comparison with **1** and other derivatives to further elucidate the mechanism of binding. All compounds except **11i** have a very high affinity around 1.0 nM and are superior to both leads **1** and **2** in this regard.

Binding Affinity to α-Synuclein and β-Amyloid. All compounds were furthermore analyzed for their binding potency toward α-synuclein and β-amyloid fibrils using well-established and validated binding assays with thioflavin-T fluorescence as read-out (for details, see Supporting Information) to determine whether structural modifications influence the selectivity of the original lead.

Because the compound library was primarily designed to produce hTau-binding compounds, we simplified the assay as much as possible and tested all compounds at three concentrations (10, 100, and 1000 nM) in triplicate for their inhibition of thioflavin binding to the fibrils. To calculate selectivity, we assumed that compounds showing less than 50% inhibition at the highest concentration of 1000 nM would have IC_{50} values >1000 nM, which could be considered as negligible. Should a significant inhibition of binding to α-synuclein or β-amyloid fibrils be observed, we would perform a concentration-dependent inhibition assay to obtain exact IC_{50} values.

For the purpose of assay validation, the aggregation of synthetic fibrils was monitored with thioflavin-T dyes for 7 days as described previously. Total binding of dye to fibrils in the absence of inhibitor was roughly 20-fold higher than nonspecific signal in the presence of a saturating concentration of LDS-798. These parameters translate to a robust assay with a pronounced effect. Studies with the reference compound LDS-798 showed concentration-dependent displacement of dye binding to α-synuclein and β-amyloid. To minimize the nonspecific signal as well as the noise from the fluorescence detection, plates were pre-read before addition of thioflavin-T to determine autofluorescence of the test solutions.

Among the novel radiotracer candidates tested, most compounds have shown very little displacement of the fluorescent dye thioflavin-T from aggregated α-synuclein. On the other hand, some binding to β-amyloid fibrils was apparent for most test compounds at the highest concentration of 1000 nM, for which a variable but low degree of displacement was observed. Values range between 9 and 32% inhibition; however, no pronounced inhibition potency was observed for any of the new entities **11a**−**v** at lower concentrations of 10 and 100 nM. With less than 50% inhibition at 1000 nM, we conclude that the IC_{50} would be >1000 nM and represent a negligible affinity toward both fibrils.

In terms of structural attributes, the binding to β-amyloid fibrils shows some correlation with the individual lipophilicity of compounds within each series. As a general trend (**11a**−**c**, **11d**−**f**, and **11g**−**i**), the lowest potency of inhibition is found in the most lipophilic analogue. A more electron-rich "azol"-heterocycle appears to benefit a lower potency as well. The trend persists within the respective series with a constant pyridine motif (**a**−**c**, **d**−**f**, and **g**−**i**). The 3-methyl-4-trifluoroethoxypyrid-2-yl-methyl residue generally produces the least potent derivative in the series. When introducing an electron-withdrawing pyrrole substituent, the trends are gravely

DOI: 10.1021/acsomega.8b00975
ACS Omega 2018, 3, 7567−7579

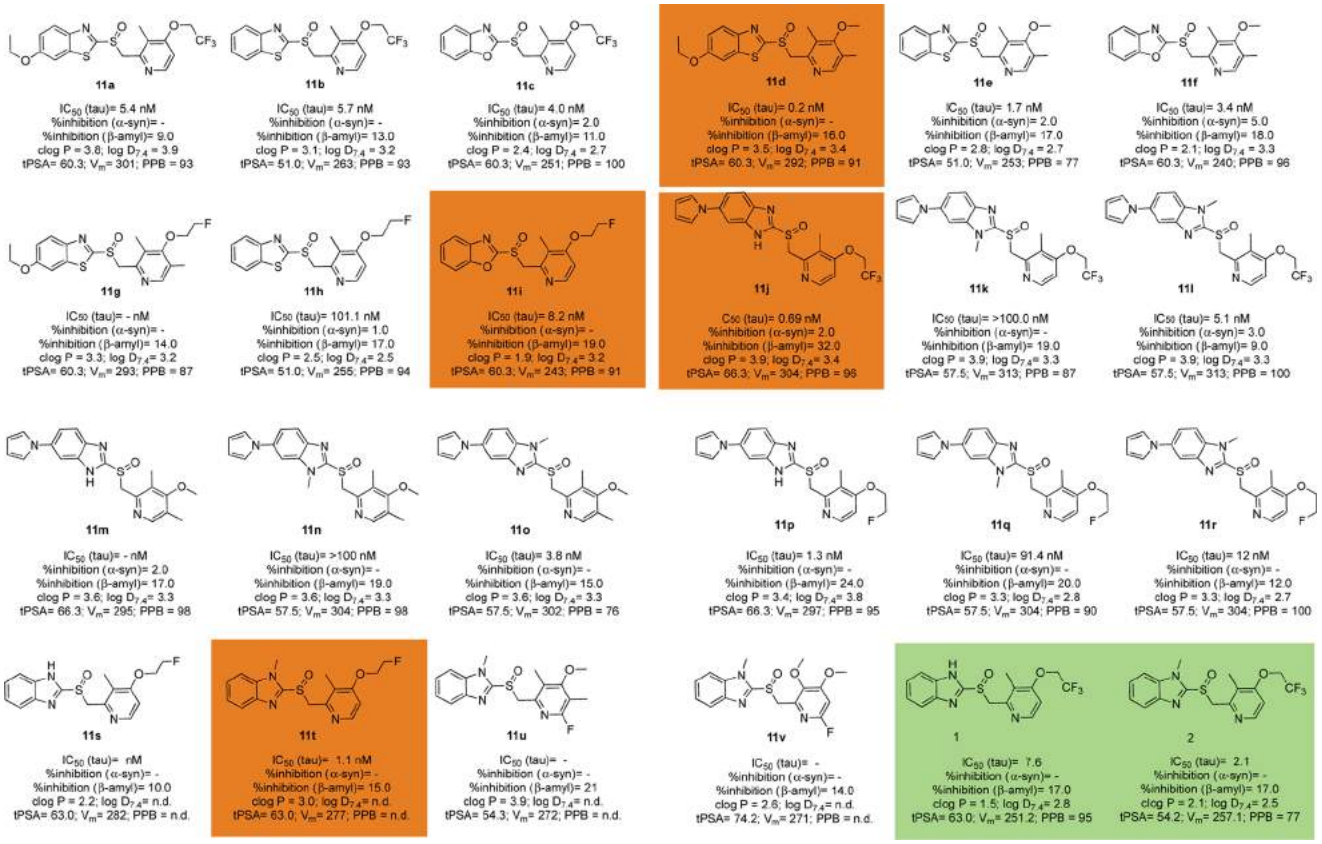

Figure 3. Molecular structures and in silico and in vitro properties of compounds **11a–v**. Reference value from the literature. IC_{50} values are given as the average of 3–9 replicates; see Supporting Information for details. Replicated twice with a broader range of concentrations. Based on single experiment, clog *P* = calculated with ChemDraw Ultra V13. Log $D_{7.4}$: decadic logarithm of the distribution coefficient between aqueous and lipid phases at pH 7.4. tPSA = topographic polar surface area, V_m = molecular volume in Å^3/mol. PPB = protein-bound fraction in percent of total concentration. n.d. = not determined. The best candidates are highlighted in orange, and lead structures 1 and 2 are highlighted in green.

affected. Interestingly, the syn-rotamer (**11l**, **11o**, and **11r**) of all *N*-methyl pyrrolobenzimidazoles is significantly less potent than the anti-rotamer (**11k**, **11n**, and **11q**), whereas the desmethyl analogues (**11j**, **11m**, and **11p**) show the most pronounced displacement, indicating some importance of the imidazole-N–H for *β*-amyloid fibril binding.

LDS-798 and **1** displaced the dye from *β*-amyloid at 1000 nM very well, which is in line with an expected strong interaction with fibrils. When tested, **1** did not show competitive inhibition of thioflavin-T binding, which is in line with (a lack of) corresponding literature evidence. We presume that astemizole binds in a different part of the misfolded protein, unlike thioflavin S and T, which are known to interact with *β*-sheet folds.

The results obtained from *α*-synuclein and *β*-amyloid binding studies indicate a low tendency of most novel candidates to bind misfolded proteins other than NFTs. These results bode for selective interaction with the target of interest, which is crucial in the development of selective PET radiotracers for NFT imaging.

We selected compounds **11i** and **11t** for further progression and **11d** and **11j** as backup as these provide the most attractive or outstanding combination of properties (Figure 3, highlighted in orange). As part of future studies, these compounds will be labeled with ^{18}F and/or ^{11}C for *μ*PET imaging studies in healthy mice and animal models of AD to prove their capacity for brain penetration and target interaction. In addition, autoradiography on healthy human tissue and samples of patients with different taupathies as well as radioligand binding assays using brain homogenates will be performed in the near future.

CONCLUSIONS

Herein, we report the lead validation of [^{18}F]lansoprazole by human PET imaging to support chemical synthesis of a small library of lansoprazole analogues designed with the aim of identifying potential radiotracer candidates for PET imaging. Compounds were designed with the aid of calculated properties, and following synthesis were successively characterized in vitro with emphasis on pharmacological criteria of relevance for brain imaging studies. Binding affinities were measured against synthetic hTau-441, *β*-amyloid, and *α*-synuclein fibrils. Lipophilicity and plasma protein binding were investigated experimentally using HPLC and membrane dialysis protocols. The data was used to gather a preliminary understanding of the structure–activity relationship for heteroarylmethyl-sulfoxides with respect to protein binding to successively optimize the lead. On the basis of the dataset, candidates **11i** and **11t** were selected for radiolabeling to allow for further progression into the preclinical imaging stage to assess the performance of new compounds as NFT imaging agents in human tissue sections and animal models. Derivatives **11d** and **11j** will be investigated in vitro and in silico to assess the importance of their structural features for binding.

DOI: 10.1021/acsomega.8b00975
ACS Omega 2018, 3, 7567–7579

EXPERIMENTAL SECTION

Materials and Methods. All chemicals, reagents, and solvents used in the experimental work were of highest commercially available quality and applied without further purification. Materials used herein were purchased from Sigma-Aldrich (Sigma-Aldrich AS, Norway), VWR (VWR International, Norway), Acros Organics (Now VWR International), Strem, ABCR, Combi-Blocks, and Fisher Scientific (Fisher Scientific AS, Oslo, Norway) unless specified here. 5-(1*H*-Pyrrol-1-yl)-2-mercaptobenzimidazole was obtained from Carbosynth (Carbosynth Limited, Berkshire, U.K.). The [^{18}F]fluoride ion for radioactive work was obtained from Norwegian Medical Cyclotron Centre AS (Gaustad, Oslo, Norway). Solid phase extraction cartridges, Sep-Pak Accell plus light QMA cartridges, and Sep-Pak C18 plus light cartridges were purchased from Waters (Waters International, Norway).

Characterization of synthesized compounds was performed using an AVIII HD 400 nuclear magnetic resonance spectrometer (Bruker ASX Nordic, Oslo, Norway). Chloroform-*d* ($CDCl_3$; δ = 7.226 ppm) was used as the reference standard. Chemical shifts (δ) for ^{1}H (400 MHz), ^{13}C (100 MHz), and ^{19}F (377 MHz) NMR are reported in parts per million (ppm). High-resolution mass spectrometry was conducted on a micromass Q-Tof-2 mass analyzer (Waters International, Oslo, Norway) and maXis II ETD (Bruker ASX Nordic, Oslo, Norway) using electron spray ionization in positive mode (ESI+). High-performance liquid chromatography (HPLC) was performed on an analytical HPLC system (Agilent technologies, California) equipped with a quaternary pump, diode array detector (DAD), and sodium iodide detector (NaI crystal; 2 × 2) using GABI-star software (Raytest, Straubenhardt, Germany) for UV and radioactive quantifications.

Chemical purity and lipophilicity ($\log D_{7.4}$) of the final compounds was determined on a Shimadzu iProminence HPLC system (Shimadzu Europa GmbH, Duisburg, Germany) using a Chromolith RP-18e column (100 × 4.6 mm^2; Merck KGaA, Darmstadt, Germany) as a stationary phase and mixtures of methanol−50 mM 3-morpholinopropane-1-sulfonic acid (MOPS) buffer, 1:1, or methanol−50 mM phosphate-buffered saline buffer, 70:30, as mobile phases with a flow rate of 2 mL/min. Complementary confirmation of the chemical purity of synthesized compounds was obtained using a pentafluorophenyl-functionalized reversed-phase column as a stationary phase (Luna PFP(2), 5 μm; 100 Å; 150 × 4.6 mm^2 column; Phenomenex, Norway) and a mixture of MeCN−H_2O, 30:70, at a flow rate of 2 mL/min as a mobile phase or using a Thermo Scientific device (Thermo Scientific UltiMate 3000 HPLC, Chromeleon) consisting of a quaternary pump, diode array detector (220 nm), and autosampler using an Ascentis Express C_{18} analytical column (150 × 4.6 mm^2, 2.7 μm particle size): eluent A: MeCN, eluent B: 0.1% formic acid, flow rate 1.0 mL/min, gradient method: 5% MeCN (0−5 min), 5−100% MeCN (5−15 min). Electrospray ionization mass spectra were obtained using a MSQ mass detector (Thermo Scientific). Thin layer chromatography (TLC) was conducted using silica gel plates (Merck KGaA, Darmstadt, Germany) with a fluorescence indicator (F_{254}) or Macherey-Nagel (Macherey-Nagel GmbH, Düren, Germany) precoated plastic sheets with fluorescent indicator UV254 (Polygram SIL G/UV254). Visualization of the spots was effected by irradiation with an UV lamp (254 and 366 nm). A miniGITA radioTLC scanner (Raytest, Straubenhardt, Germany) was used for the detection of radioTLC spots. Radioactivity measurements were performed with an Atomlab 300 dose calibrator (Biodex medical systems Inc.) and activity is reported in Becquerel (Bq, s^{-1}).

Radiochemistry. All reagents, solvents, and reference compound **1** were purchased from Merck Millipore or Sigma-Aldrich in pharmaceutical grade. Difluorovinyl precursors for **1** (2-(((5-((2,2-difluorovinyl)oxy)-3-methylpyridin-2-yl)-methyl)sulfinyl)-1*H*-benzo[*d*]imidazole) (**3a**) and **2** (2-(((4-((2,2-difluorovinyl)oxy)-3-methylpyridin-2-yl)-methyl)-sulfinyl)-1-methyl-1*H*-benzo[*d*]imidazole) (**3b**) were prepared as described previously. [^{18}F]Fluoride ([^{18}F]F$^-$) was produced via the ^{18}O(p,n)^{18}F nuclear reaction using an IBA Cyclone 18/9 cyclotron.

General Procedure for Synthesis of Compounds 10a−v. 2-Merceptobenzoxa- and -thiazoles, **9a−e** (1.1 equiv), were treated with a solution of NaOH (3 equiv) in H_2O (10 mL) for 10 min at room temperature (rt). Respective pyridine building blocks, **8a−f** (1.0 equiv), were dissolved separately in H_2O (2 mL) and added slowly to the reaction mixture. Precipitate formation was observed immediately on addition, and reaction contents were allowed to stir for 1 h at rt. The reaction mixture was extracted with dichloromethane (3 × 20 mL) and the organic layers were combined, dried over Na_2SO_4, and concentrated in vacuo to obtain the respective sulfides (**10a−v**).

General Procedure for Synthesis of Compounds 11a−v. Oxidation of sulfide intermediates **10a−v** (1.0 equiv) was achieved using portions of *meta*-chloroperbenzoic acid (*m*-CPBA, 1.1 equiv) in $CHCl_3$ (8−10 mL) at 0 °C for 30 min. The reaction was quenched with $NaHCO_3$ (10 mL) and extracted with dichloromethane (DCM) (3 × 10 mL). The organic extracts were combined, washed with brine (20 mL), and dried over Na_2SO_4 to obtain the crude product. The product was purified by column chromatography on silica gel with MeOH−DCM, 1:9, to isolate the respective sulfoxides (**11a−v**).

*6-Ethoxy-2-(((3-methyl-4-(2,2,2-trifluoroethoxy)pyridin-2-yl)methyl)thio)benzothiazol (**10a**) (403 mg, 97%).* ^{1}H NMR (400 MHz, $CDCl_3$) δ 8.36 (d, J = 5.6 Hz, 1H), 7.77 (d, J = 9.0 Hz, 1H), 7.22 (d, J = 2.5 Hz, 1H), 7.01 (dd, J = 9.0, 2.5 Hz, 1H), 6.65 (d, J = 5.6 Hz, 1H), 4.78 (s, 2H), 4.40 (q, J = 7.8 Hz, 2H), 4.07 (q, J = 7.0 Hz, 2H), 2.35 (s, 3H), 1.41 (t, J = 7.0 Hz, 3H); ^{13}C NMR (100 MHz, $CDCl_3$) δ 163.1, 161.8, 156.6, 155.9, 148.3, 147.8, 137.0, 122.2, 121.7, 115.4, 105.7, 105.0, 65.5 (q, $^2J_{CF}$ = 36.7 Hz), 64.3, 38.2, 14.9, 10.9; ^{19}F NMR (377 MHz, $CDCl_3$) δ −73.85 (s, 3F).

*6-Ethoxy-2-(((3-methyl-4-(2,2,2-trifluoroethoxy)pyridin-2-yl)methyl)sulfinyl)benzothiazole (**11a**).* (136 mg, 36%) ^{1}H NMR (400 MHz, $CDCl_3$) δ 8.33 (d, J = 5.6 Hz, 1H), 7.92 (d, J = 9.0 Hz, 1H), 7.39 (d, J = 2.5 Hz, 1H), 7.14 (dd, J = 9.0, 2.5 Hz, 1H), 6.67 (d, J = 5.6 Hz, 1H), 4.68 (s, 2H), 4.40 (q, J = 7.8 Hz, 2H), 4.12 (q, J = 7.0 Hz, 2H), 2.25 (s, 3H), 1.48 (t, J = 7.0 Hz, 3H); ^{13}C NMR (100 MHz, $CDCl_3$) δ 173.2, 161.9, 157.9, 150.7, 148.6, 148.2, 137.8, 124.7, 123.6, 117.4, 106.0, 104.8, 65.5 (q, $^2J_{CF}$ = 36.7 Hz), 64.3, 63.1, 14.9, 11.2; ^{19}F NMR (377 MHz, $CDCl_3$) δ −73.79 (s, 3F); IR (KBr) ν (in cm^{-1}) 3028 (sp^2 C−H stretching), 2935 (sp^3 C−H stretching), 1604 (C═N stretching), 1580, 1475 (C═C stretching), 1447, 1395, 1256, 1212, 1110 (S═O stretching), 1053, 991 (C−O stretching), 938, 855, 800, 716, 658, 569; high-resolution mass spectrometry (HR-MS) (ESI) m/z calcd for

DOI: 10.1021/acsomega.8b00975
ACS Omega 2018, 3, 7567−7579

$C_{18}H_{17}F_3N_2O_3S_2$, 430.0633; found, 431.0719 $(M + H)^+$; HPLC >98%.

*2-(((3-Methyl-4-(2,2,2-trifluoroethoxy)pyridin-2-yl)-methyl)thio)benzothiazole (**10b**) (351 mg, 95%).* ^{1}H NMR (400 MHz, $CDCl_3$) δ 8.32 (d, J = 5.7 Hz, 1H), 8.02 (d, J = 8.0 Hz, 1H), 7.88 (d, J = 8.1 Hz, 1H), 7.47 (dtd, J = 15.5, 7.2, 1.2 Hz, 1H), 7.37 (dtd, J = 15.3, 7.2, 1.3 Hz, 1H), 7.11 (d, J = 5.6 Hz, 1H), 4.91 (q, J = 7.8 Hz, 2H), 4.83 (s, 2H), 2.27 (s, 3H); ^{13}C NMR (100 MHz, $CDCl_3$) δ 167.8, 162.3, 152.6, 150.1, 147.9, 135.7, 126.7, 125.5, 123.1, 122.6, 121.1, 105.3, 65.6 (q, $^2J_{CF}$ = 36.7 Hz), 38.1, 11.2; ^{19}F NMR (377 MHz, $CDCl_3$) δ −73.83 (s, 3F).

*2-(((3-Methyl-4-(2,2,2-trifluoroethoxy)pyridin-2-yl)-methyl)sulfinyl)benzothiazole (**11b**) (88 mg, 26%).* ^{1}H NMR (400 MHz, $CDCl_3$) δ 8.33 (d, J = 5.6 Hz, 1H), 8.07 (d, J = 8.1 Hz, 1H), 8.01 (d, J = 8.1 Hz, 1H), 7.57 (dtd, J = 15.5, 7.2, 1.2 Hz, 1H), 7.50 (dtd, J = 15.3, 7.2, 1.3 Hz, 1H), 6.68 (d, J = 5.6 Hz, 1H), 4.75−4.66 (m, 2H), 4.40 (q, J = 7.8 Hz, 2H), 2.26 (s, 3H); ^{13}C NMR (100 MHz, $CDCl_3$) δ 177.2, 161.9, 153.8, 150.6, 148.6, 136.2, 127.0, 126.3, 124.2, 123.6, 122.4, 106.1, 65.5 (q, $^2J_{CF}$ = 36.7 Hz), 63.0, 11.2; ^{19}F NMR (377 MHz, $CDCl_3$) δ −73.78 (s, 3F); IR (KBr) ν (in cm^{-1}) 3059 (sp^2 C−H stretching), 2932 (sp^3 C−H stretching), 1583 (C═N stretching), 1474 (C═C stretching), 1432, 1393, 1261, 1078 (S═O stretching), 1050, 981 (C−O stretching), 866, 796, 764, 730, 680, 597; HR-MS (ESI) m/z calcd for $C_{16}H_{13}F_3N_2O_2S_2$, 386.0371; found, 387.0458 $(M + H)^+$; HPLC >98%.

*2-(((3-Methyl-4-(2,2,2-trifluoroethoxy)pyridin-2-yl)-methyl)thio)benzoxazole (**10c**) (241 mg, 90%).* ^{1}H NMR (400 MHz, $CDCl_3$) δ 8.40 (d, J = 5.6 Hz, 1H), 7.62 (d, J = 8.0 Hz, 1H), 7.45 (d, J = 8.0 Hz, 1H), 7.27 (ddd, J = 15.2, 7.4, 1.2 Hz, 2H), 6.69 (d, J = 5.6 Hz, 1H), 4.81 (s, 2H), 4.41 (q, J = 7.8 Hz, 2H), 2.37 (s, 3H); ^{13}C NMR (100 MHz, $CDCl_3$) δ 168.6, 164.9, 155.0, 152.1, 148.1, 142.0, 133.2, 130.2, 124.4, 118.6, 110.1, 105.9, 66.6 (q, $^2J_{CF}$ = 36.6 Hz), 36.7, 10.9; ^{19}F NMR (377 MHz, $CDCl_3$) δ −73.83 (s, 3F).

*2-(((3-Methyl-4-(2,2,2-trifluoroethoxy)pyridin-2-yl)-methyl)sulfinyl)benzooxazole (**11c**) (54 mg, 23%).* ^{1}H NMR (400 MHz, $CDCl_3$) δ 8.22 (d, J = 5.6 Hz, 1H), 7.82 (d, J = 8.0 Hz, 1H), 7.65 (d, J = 8.0 Hz, 1H), 7.45 (ddd, J = 15.2, 7.4, 1.2 Hz, 2H), 6.64 (d, J = 5.6 Hz, 1H), 4.87 (s, 2H), 4.38 (q, J = 7.8 Hz, 2H), 2.31 (s, 3H); ^{13}C NMR (100 MHz, $CDCl_3$) δ 164.6, 161.9, 151.8, 150.4, 148.6, 140.6, 127.1, 125.6, 123.6, 121.4, 111.6, 106.1, 66.5 (q, $^2J_{CF_3}$ = 36.6 Hz), 59.7, 11.2; ^{19}F NMR (377 MHz, $CDCl_3$) δ −73.79 (s, 3F); IR (KBr) ν (in cm^{-1}) 3014 (sp^2 C−H stretching), 2930 (sp^3 C−H stretching), 1580 (C═N stretching), 1479 (C═C stretching), 1306, 1261, 1168, 1103 (S═O stretching), 1047, 938 (C−O stretching), 878, 833, 759, 677, 608, 583; HR-MS (ESI) m/z calcd for $C_{16}H_{13}F_3N_2O_3S$, 370.0599; found, 371.0687 $(M + H)^+$; HPLC >98%.

*6-Ethoxy-2-(((4-methoxy-3,5-dimethylpyridin-2-yl)-methyl)thio)benzo[d]thiazole (**10d**) (305 mg, 85%).* ^{1}H NMR (400 MHz, $CDCl_3$) δ 8.23 (s, 1H), 7.76 (d, J = 9.0 Hz, 1H), 7.23 (d, J = 2.5 Hz, 1H), 7.01 (dd, J = 9.0, 2.5 Hz, 1H), 4.62 (s, 2H), 4.11 (q, J = 7.0 Hz, 2H), 3.68 (s, 3H), 2.35 (s, 3H), 2.16 (s, 3H), 1.40 (t, J = 7.0 Hz, 3H); ^{13}C NMR (100 MHz, $CDCl_3$) δ 167.7, 164.3, 156.5, 154.3, 148.1, 147.6, 137.0, 126.1, 124.9, 122.2, 119.1, 104.3, 64.5, 62.9, 36.2, 14.8, 13.6, 10.9.

*6-Ethoxy-2-(((4-methoxy-3,5-dimethylpyridin-2-yl)-methyl)sulfinyl)benzothiazole (**11d**) (102 mg, 34%).* ^{1}H NMR (400 MHz, $CDCl_3$) δ 8.21 (s, 1H), 7.91 (d, J = 9.0 Hz, 1H), 7.39 (d, J = 2.5 Hz, 1H), 7.13 (dd, J = 9.0, 2.5 Hz, 1H), 4.63 (s, 2H), 4.11 (q, J = 7.0 Hz, 2H), 3.72 (s, 3H), 2.24 (s, 3H), 2.22 (s, 3H), 1.47 (t, J = 7.0 Hz, 3H); ^{13}C NMR (100 MHz, $CDCl_3$) δ 173.4, 164.3, 157.9, 150.0, 148.8, 148.2, 137.8, 127.2, 126.3, 124.7, 117.3, 104.8, 64.3, 63.3, 60.1, 14.9, 13.5, 11.8; IR (KBr) ν (in cm^{-1}) 3017 (sp^2 C−H stretching), 2904 (sp^3 C−H stretching), 1598 (C═N stretching), 1468 (C═C stretching), 1443, 1397, 1250, 1222, 1079 (S═O stretching), 1042, 983 (C−O stretching), 928, 822, 782, 687, 611, 555; HR-MS (ESI) m/z calcd for $C_{18}H_{20}N_2O_3S_2$, 376.0915; found, 377.1006 $(M + H)^+$; HPLC >98%.

*2-(((4-Methoxy-3,5-dimethylpyridin-2-yl)methyl)thio)-benzothiazole (**10e**) (308 mg, 97%).* ^{1}H NMR (400 MHz, $CDCl_3$) δ 8.22 (s, 1H), 7.89 (d, J = 8.1 Hz, 1H), 7.75 (d, J = 8.0 Hz, 1H), 7.41 (dtd, J = 15.5, 7.2, 1.1 Hz, 1H), 7.29 (dtd, J = 15.4, 7.2, 1.1 Hz, 1H), 4.79 (s, 2H), 3.77 (s, 3H), 2.37 (s, 3H), 2.25 (s, 3H); ^{13}C NMR (101 MHz, $CDCl_3$) δ 166.9, 164.3, 153.7, 153.3, 149.5, 135.6, 126.1, 125.8, 125.4, 124.3, 121.6, 121.1, 60.1, 38.1, 13.4, 11.5.

*2-(((4-Methoxy-3,5-dimethylpyridin-2-yl)methyl)sulfinyl)-benzothiazol (**11e**) (92 mg, 31%).* ^{1}H NMR (400 MHz, $CDCl_3$) δ 8.21 (s, 1H), 8.06 (d, J = 8.1 Hz, 1H), 8.00 (d, J = 8.1 Hz, 1H), 7.56 (dtd, J = 15.5, 7.2, 1.1 Hz, 1H), 7.49 (dtd, J = 15.4, 7.2, 1.1 Hz, 1H), 4.70−4.61 (m, 2H), 3.73 (s, 3H), 2.25 (s, 3H), 2.23 (s, 3H); ^{13}C NMR (101 MHz, $CDCl_3$) δ 177.4, 164.3, 153.8, 150.0, 148.8, 136.2, 127.2, 127.0, 126.4, 126.3, 124.2, 122.4, 63.3, 60.1, 13.5, 11.8; IR (KBr) ν (in cm^{-1}) 3047 (sp^2 C−H stretching), 2940 (sp^3 C−H stretching), 1567 (C═N stretching), 1465 (C═C stretching), 1426, 1402, 1272, 1086 (S═O stretching), 1043, 996 (C−O stretching), 873, 791, 759, 726, 669, 588; HR-MS (ESI) m/z calcd for $C_{16}H_{16}N_2O_2S_2$, 332.0653; found, 333.0741 $(M + H)^+$; HPLC >98%.

*2-(((4-Methoxy-3,5-dimethylpyridin-2-yl)methyl)thio)-benzoxazole (**10f**) (207 mg, 92%).* ^{1}H NMR (400 MHz, $CDCl_3$) δ 8.22 (s, 1H), 7.62 (d, J = 7.7 Hz, 1H), 7.45 (d, J = 7.8 Hz, 1H), 7.26 (dddddd, J = 15.3, 7.3, 1.0 Hz, 2H), 4.75 (s, 2H), 3.77 (s, 3H), 2.37 (s, 3H), 2.25 (s, 3H); ^{13}C NMR (101 MHz, $CDCl_3$) δ 165.3, 164.2, 153.1, 152.0, 149.5, 142.1, 125.9, 125.2, 124.3, 124.0, 118.5, 110.0, 60.1, 37.3, 13.4, 11.5.

*2-(((4-Methoxy-3,5-dimethylpyridin-2-yl)methyl)sulfinyl)-benzooxazole (**11f**) (42 mg, 21%).* ^{1}H NMR (400 MHz, $CDCl_3$) δ 8.05 (s, 1H), 7.58 (d, J = 7.7 Hz, 1H), 7.41 (d, J = 7.8 Hz, 1H), 7.26 (dddddd, J = 15.3, 7.3, 1.0 Hz, 2H), 4.86 (s, 2H), 3.74 (s, 3H), 2.52 (s, 3H), 2.22 (s, 3H); ^{13}C NMR (100 MHz, $CDCl_3$) δ 166.6, 155.8, 152.3, 145.8, 141.9, 138.2, 128.7, 128.5, 124.3, 123.9, 118.3, 110.1, 60.6, 29.9, 13.5, 12.6; IR (KBr) ν (in cm^{-1}) 3021 (sp^2 C−H stretching), 2923 (sp^3 C−H stretching), 1573 (C═N stretching), 1472 (C═C stretching), 1315, 1249, 1170, 1110 (S═O stretching), 1043, 972 (C−O stretching), 862, 815, 748, 663, 601, 576; HR-MS (ESI) m/z calcd for $C_{16}H_{16}N_2O_3S$, 316.0882; found, 317.0968 $(M + H)^+$; HPLC >98%.

*6-Ethoxy-2-(((4-(2-fluoroethoxy)-3-methylpyridin-2-yl)-methyl)thio)benzodthiazole (**10g**) (174 mg, 92%).* ^{1}H NMR (400 MHz, $CDCl_3$) δ 8.30 (d, J = 5.6 Hz, 1H), 7.76 (d, J = 9.0 Hz, 1H), 7.21 (d, J = 2.4 Hz, 1H), 6.99 (dd, J = 9.0, 2.5 Hz, 1H), 6.66 (d, J = 5.6 Hz, 1H), 4.88−4.83 (m, 1H), 4.76 (s, 2H), 4.72−4.68 (m, 1H), 4.31−4.27 (m, 1H), 4.22−4.17 (m, 1H), 4.05 (q, J = 7.0 Hz, 2H), 2.32 (s, 3H), 1.43 (t, J = 7.0 Hz,

DOI: 10.1021/acsomega.8b00975
ACS Omega 2018, 3, 7567−7579

3H); ^{13}C NMR (100 MHz, $CDCl_3$) δ 167.1, 161.8, 156.1, 147.9, 147.2, 146.7, 137.1, 125.1, 124.7, 118.2, 105.8, 104.2, 82.2 (d, $^1J_{CF}$ = 172.3 Hz), 67.4 (d, $^2J_{CF}$ = 20.7 Hz), 63.8, 37.5, 14.6, 11.1.

*6-Ethoxy-2-(((4-(2-fluoroethoxy)-3-methylpyridin-2-yl)-methyl)sulfinyl)benzothiazole (**11g**) (43 mg, 31%).* ^{1}H NMR (400 MHz, $CDCl_3$) δ 8.29 (d, J = 5.6 Hz, 1H), 7.92 (d, J = 9.0 Hz, 1H), 7.39 (d, J = 2.4 Hz, 1H), 7.13 (dd, J = 9.0, 2.5 Hz, 1H), 6.69 (d, J = 5.6 Hz, 1H), 4.84 (t, J = 4.1 Hz, 3H), 4.73 (t, J = 4.0 Hz, 3H), 4.67 (s, 2H), 4.31−4.28 (m, 1H), 4.24−4.21 (m, 1H), 4.12 (q, J = 7.0 Hz, 2H), 2.24 (s, 3H), 1.47 (t, J = 7.0 Hz, 3H); ^{13}C NMR (100 MHz, $CDCl_3$) δ 173.4, 163.1, 157.9, 150.0, 148.5, 148.2, 137.9, 124.7, 123.3, 117.3, 106.1, 104.8, 82.5 (d, $^1J_{CF}$ = 172.3 Hz), 67.4 (d, $^2J_{CF}$ = 20.7 Hz), 64.3, 63.3, 14.9, 11.3; IR (KBr) ν (in cm^{-1}) 2987 (sp^2 C−H stretching), 2917 (sp^3 C−H stretching), 1599 (C═N stretching), 1472, 1445 (C═C stretching), 1296, 1253, 1221, 1085 (S═O stretching), 1050, 940 (C−O stretching), 883, 818, 725, 681, 606, 558; HR-MS (ESI) m/z calcd for $C_{18}H_{19}FN_2O_3S_2$, 394.0821; found, 395.0892 (M + H)$^+$; HPLC >98%.

*2-(((4-(2-Fluoroethoxy)-3-methylpyridin-2-yl)methyl)-thio)benzothiazole (**10h**) (147 mg, 88%).* ^{1}H NMR (400 MHz, $CDCl_3$) δ 8.32 (d, J = 5.7 Hz, 1H), 7.89 (d, J = 8.2 Hz, 1H), 7.75 (d, J = 8.1 Hz, 1H), 7.41 (dtd, J = 15.5, 7.1, 1.1 Hz, 1H), 7.29 (dtd, J = 15.3, 7.2, 1.1 Hz, 1H), 6.68 (d, J = 5.7 Hz, 1H), 4.86−4.83 (m, 1H), 4.82 (s, 2H), 4.74−4.71 (m, 1H), 4.30−4.27 (m, 1H), 4.23−4.20 (m, 1H), 2.34 (s, 3H); ^{13}C NMR (100 MHz, $CDCl_3$) δ 166.9, 161.3, 155.4, 150.6, 147.6, 135.9, 126.1, 125.8, 124.6, 123.1, 122.1, 106.6, 81.5 (d, $^1J_{CF}$ = 172 Hz), 67.3 (d, $^2J_{CF}$ = 20.7 Hz), 38.5, 10.8.

*2-(2-(((4-(2-Fluoroethoxy)-3-methylpyridin-2-yl)methyl)-sulfinyl)benzothiazole) (**11h**) (37 mg, 32%).* ^{1}H NMR (400 MHz, $CDCl_3$) δ 8.30 (d, J = 5.7 Hz, 1H), 8.07 (d, J = 8.2 Hz, 1H), 8.00 (d, J = 8.1 Hz, 1H), 7.56 (dtd, J = 15.5, 7.1, 1.1 Hz, 1H), 7.49 (dtd, J = 15.3, 7.2, 1.1 Hz, 1H), 6.70 (d, J = 5.7 Hz, 1H), 4.85 (t, J = 4.1 Hz, 3H), 4.73 (t, J = 4.0 Hz, 3H), 4.74−4.65 (m, 2H), 4.32−4.28 (m, 1H), 4.25−4.21 (m, 1H), 2.25 (s, 3H); ^{13}C NMR (100 MHz, $CDCl_3$) δ 177.5, 163.1, 153.9, 149.9, 148.5, 136.3, 127.0, 126.3, 124.2, 123.3, 122.4, 106.1, 81.5 (d, $^1J_{CF}$ = 172 Hz), 67.4 (d, $^2J_{CF}$ = 20.7 Hz), 63.3, 11.3; IR (KBr) ν (in cm^{-1}) 3011 (sp^2 C−H stretching), 2937 (sp^3 C−H stretching), 1580 (C═N stretching), 1475, 1423 (C═C stretching), 1299, 1233, 1103 (S═O stretching), 1047, 948 (C−O stretching), 885, 829, 739, 690, 586, 547; HR-MS (ESI) m/z calcd for $C_{16}H_{15}FN_2O_2S_2$, 350.0559; found, 351.0630 (M + H)$^+$; HPLC >98%.

*2-(((4-(2-Fluoroethoxy)-3-methylpyridin-2-yl)methyl)-thio)benzoxazole (**10i**) (146 mg, 92%).* ^{1}H NMR (400 MHz, $CDCl_3$) δ 8.32 (d, J = 7.2 Hz, 1H), 7.39 (d, J = 7.7 Hz, 1H), 7.23 (d, J = 7.6 Hz, 1H), 7.11 (dddddd, J = 7.6, 1.2 Hz, 2H), 6.78 (d, J = 7.1 Hz, 1H), 4.86 (s, 2H), 4.84−4.80 (m, 1H), 4.72−4.68 (m, 1H), 4.30−4.27 (m, 1H), 4.23−4.20 (m, 1H), 2.56 (s, 3H); ^{13}C NMR (100 MHz, $CDCl_3$) δ 168.9, 164.9, 158.6, 154.4, 149.6, 142.3, 139.2, 125.2, 124.2, 123.3, 119.7, 111.3, 108.6, 81.2 (d, $^1J_{CF}$ = 172 Hz), 68.3 (d, $^2J_{CF}$ = 20.4 Hz), 57.2, 11.1.

*2-(((4-(2-Fluoroethoxy)-3-methylpyridin-2-yl)methyl)-sulfinyl)benzoxazole (**11i**) (37 mg, 27%).* ^{1}H NMR (400 MHz, $CDCl_3$) δ 8.16 (d, J = 7.2 Hz, 1H), 7.58 (d, J = 7.7 Hz, 1H), 7.42 (d, J = 7.6 Hz, 1H), 7.25 (dd, J = 7.6, 1.2 Hz, 2H), 6.73 (d, J = 7.1 Hz, 1H), 4.91 (s, 2H), 4.86−4.81 (m, 1H), 4.74−4.69 (m, 1H), 4.31−4.26 (m, 1H), 4.24−4.20 (m, 1H), 2.52 (s, 3H); ^{13}C NMR (100 MHz, $CDCl_3$) δ 166.4, 155.0, 152.3, 147.9, 141.9, 137.1, 124.7, 124.3, 123.9, 118.4, 110.1, 107.3, 81.3 (d, $^1J_{CF}$ = 172.8 Hz), 68.2 (d, $^2J_{CF}$ = 20.4 Hz), 37.8, 12.3; IR (KBr) ν (in cm^{-1}) 3021 (sp^2 C−H stretching), 2913 (sp^3 C−H stretching), 1587 (C═N stretching), 1468, 1431 (C═C stretching), 1289, 1226, 1098 (S═O stretching), 1034, 946 (C−O stretching), 878, 811, 738, 692, 611, 571; HR-MS (ESI) m/z calcd for $C_{16}H_{15}FN_2O_3S$, 334.0787; found, 335.0859 (M + H)$^+$; HPLC >98%.

*2-(((3-Methyl-4-(2,2,2-trifluoroethoxy)pyridin-2-yl)-methyl)thio)-5-(1H-pyrrol-1-yl)-1H-benzoimidazole (**10j**) (178 mg, 85%).* ^{1}H NMR (400 MHz, $CDCl_3$) δ 12.37 (br s, 1H), 8.32 (d, J = 5.6 Hz, 1H), 8.07−7.50 (m, 2H), 7.39 (dd, J = 8.7, 2.1 Hz, 1H), 7.09 (t, J = 2.1 Hz, 2H), 6.61 (d, J = 5.6 Hz, 1H), 6.38 (t, J = 2.2 Hz, 2H), 4.89−4.74 (m, 2H), 4.30 (qd, J = 7.8, 5.2 Hz, 2H), 2.20 (s, 3H); ^{13}C NMR (100 MHz, $CDCl_3$) δ 163.0, 157.2, 147.3, 136.8, 121.5, 120.3, 115.9, 110.1, 106.3, 79.2, 65.5 (q, $^2J_{CF}$ = 36.3 Hz), 37.6, 10.8; ^{19}F NMR (377 MHz, $CDCl_3$) δ −73.78 (s, 3F).

*2-(((3-Methyl-4-(2,2,2-trifluoroethoxy)pyridin-2-yl)-methyl)sulfinyl)-5-(1H-pyrrol-1-yl)-1H-benzoimidazole (**11j**) (54 mg, 33%).* ^{1}H NMR (400 MHz, $CDCl_3$) δ 12.47 (br s, 1H), 8.31 (d, J = 5.6 Hz, 1H), 7.85−7.52 (m, 2H), 7.38 (dd, J = 8.7, 2.1 Hz, 1H), 7.09 (t, J = 2.1 Hz, 2H), 6.60 (d, J = 5.6 Hz, 1H), 6.38 (t, J = 2.2 Hz, 2H), 4.81 (q, J = 13.9 Hz, 2H), 4.29 (p, J = 8.0 Hz, 2H), 2.18 (s, 3H); ^{13}C NMR (100 MHz, $CDCl_3$) δ 161.9, 150.4, 148.5, 123.4, 120.1, 110.5, 106.2, 77.1, 65.4 (q, $^2J_{CF}$ = 36.3 Hz), 60.8, 11.10; ^{19}F NMR (377 MHz, $CDCl_3$) δ −73.77 (s, 3F); IR (KBr) ν (in cm^{-1}) 3310 (N−H stretching), 2961 (sp^2 C−H stretching), 2810 (sp^3 C−H stretching), 1630, 1580 (C═N stretching), 1513, 1485 (C═C stretching), 1411, 1317, 1258, 1166, 1110 (S═O stretching), 1046, 969 (C−O stretching), 892, 854, 808, 730, 663, 604, 576; HR-MS (ESI) m/z calcd for $C_{20}H_{17}F_3N_4O_2S$, 434.1024; found, 457.0913 (M + Na)$^+$; HPLC >98%.

*1-Methyl-2-(((3-methyl-4-(2,2,2-trifluoroethoxy)pyridin-2-yl)methyl)sulfinyl)-5-(1H-pyrrol-1-yl)-1H-benzoimidazole (**11k**) (47 mg, 23%).* ^{1}H NMR (400 MHz, $CDCl_3$) δ 8.23 (d, J = 5.6 Hz, 1H), 7.83 (d, J = 8.7 Hz, 1H), 7.41 (dd, J = 8.7, 2.1 Hz, 1H), 7.36 (d, J = 2.0 Hz) 7.13 (t, J = 2.2 Hz, 2H), 6.63 (d, J = 5.7 Hz, 1H), 6.39 (t, J = 2.2 Hz, 2H), 5.07−4.94 (m, 2H), 4.38 (q, J = 7.8 Hz, 2H), 4.03 (s, 3H), 2.32 (s, 3H), ^{13}C NMR (100 MHz, $CDCl_3$) δ 161.8, 153.0, 151.5, 148.3, 140.3, 138.4, 137.1, 124.3, 123.3, 122.1, 120.1, 117.8, 110.8, 105.9, 102.0, 66.5 (q, $^2J_{CF}$ = 36.6 Hz), 59.3, 31.0, 11.1; ^{19}F NMR (377 MHz, $CDCl_3$) δ −73.76 (s, 3F); IR (KBr) ν (in cm^{-1}) 3457 (N−H stretching), 3111 (sp^2 C−H stretching), 2953 (sp^3 C−H stretching), 1618, 1584 (C═N stretching), 1497, 1464 (C═C stretching), 1367, 1308, 1269, 1157, 1114 (S═O stretching), 1051, 979 (C−O stretching), 879, 813, 741, 664, 639, 611, 578; HR-MS (ESI) m/z calcd for $C_{21}H_{19}F_3N_4O_2S$, 448.1181; found, 471.1109 (M + Na)$^+$; HPLC >98%.

*1-Methyl-2-(((3-methyl-4-(2,2,2-trifluoroethoxy)pyridin-2-yl)methyl)sulfinyl)-5-(1H-pyrrol-1-yl)-1H-benzoimidazole (**11l**) (28 mg, 11%).* ^{1}H NMR (400 MHz, $CDCl_3$) δ 8.22 (d, J = 5.7 Hz, 1H), 7.80 (d, J = 1.8 Hz, 1H), 7.49−7.43 (m, 2H), 7.11 (t, J = 2.2 Hz, 2H), 6.63 (d, J = 5.6 Hz, 1H), 6.37 (t, J = 2.2 Hz, 2H), 5.07−4.95 (m, 2H), 4.38 (q, J = 7.8 Hz, 2H), 4.05 (s, 3H), 2.32 (s, 3H); ^{13}C NMR (100 MHz, $CDCl_3$) δ 161.8, 153.6, 151.4, 148.2, 142.7, 137.4, 134.8, 123.3, 120.1, 119.1, 112.9, 110.7, 110.5, 105.9, 65.4 (q, $^2J_{CF}$ = 36.2 Hz), 59.3, 31.0, 11.1; ^{19}F NMR (377 MHz, $CDCl_3$) δ −73.75 (s, 3F); IR (KBr) ν (in cm^{-1}) 3460 (N−H stretching), 3108 (sp^2 C−H stretching), 2947 (sp^3 C−H stretching), 1627, 1578

DOI: 10.1021/acsomega.8b00975
ACS Omega 2018, 3, 7567−7579

(C═N stretching), 1503, 1475 (C═C stretching), 1373, 1310, 1264, 1163, 1110 (S═O stretching), 1043, 976 (C−O stretching), 885, 818, 734, 660, 633, 614, 573; HR-MS (ESI) m/z calcd for $C_{21}H_{19}F_3N_4O_2S$, 448.1181; found, 471.1109 $(M + Na)^+$; HPLC >96%.

*2-(((4-Methoxy-3,5-dimethylpyridin-2-yl)methyl)thio)-5-(1H-pyrrol-1-yl)-1H-benzoimidazole (**10k**) (523 mg, 96%).* ^{1}H NMR (400 MHz, $CDCl_3$) δ 12.37 (br s, 1H), δ 8.13 (s, 1H), 7.52 (d, J = 8.8 Hz, 2H), 7.32 (dd, J = 8.6, 2.1 Hz, 1H), 7.13 (t, J = 2.2 Hz, 2H), 6.27 (t, J = 2.2 Hz, 2H), 4.60 (s, 2H), 3.77 (s, 3H), 2.31 (s, 3H), 2.24 (s, 3H); ^{13}C NMR (100 MHz, $CDCl_3$) δ 166.3, 155.3, 149.8, 138.0, 127.7, 127.2, 120.7, 111.0, 60.6, 37.5, 13.4, 11.3.

*2-(((4-Methoxy-3,5-dimethylpyridin-2-yl)methyl)sulfinyl)-5-(1H-pyrrol-1-yl)-1H-benzo[d]imidazole (**11m**) (263 mg, 51%).* ^{1}H NMR (400 MHz, $CDCl_3$) δ 12.57 (br s, 1H), 8.18 (s, 1H), 7.88−7.36 (m, 2H), 7.37 (dd, J = 8.7, 2.1 Hz, 1H), 7.09 (t, J = 2.2 Hz, 2H), 6.37 (t, J = 2.1 Hz, 2H), 4.82−4.73 (m, 2H), 3.62 (s, 3H), 2.18 (d, J = 4.3 Hz, 6H); ^{13}C NMR (100 MHz, $CDCl_3$) δ 164.5, 149.8, 148.6, 127.0, 126.7, 120.1, 110.5, 60.8, 60.0, 13.4, 11.6; IR (KBr) ν (in cm^{-1}) 3357 (N−H stretching), 3098 (sp^2 C−H stretching), 2982 (sp^3 C−H stretching), 1632, 1587 (C═N stretching), 1517, 1480 (C═C stretching), 1423, 1359, 1271, 1212, 1078 (S═O stretching), 997, 969 (C−O stretching), 889, 848, 801, 720, 615, 607, 581; HR-MS (ESI) m/z calcd for $C_{20}H_{20}N_4O_2S$, 380.1307; found, 403.1199 $(M + Na)^+$; HPLC >98%.

*1-Methyl-2-(((3-methyl-4-(2,2,2-trifluoroethoxy)pyridin-2-yl)methyl)sulfinyl)-5-(1H-pyrrol-1-yl)-1H-benzo[d]imidazole (**11n**) (43 mg, 24%).* ^{1}H NMR (400 MHz, $CDCl_3$) δ 8.09 (s, 1H), 7.83 (d, J = 8.7 Hz, 1H), 7.41 (dd, J = 8.7, 2.1 Hz, 1H), 7.35 (d, J = 2.0 Hz, 1H), 7.13 (t, J = 2.2 Hz, 2H), 6.38 (t, J = 2.1 Hz, 2H), 5.02−4.88 (m, 2H), 3.99 (s, 3H), 3.70 (s, 3H), 2.29 (s, 3H), 2.20 (s, 3H); ^{13}C NMR (100 MHz, $CDCl_3$) δ 164.4, 153.3, 149.7, 149.5, 140.3, 138.3, 137.1, 126.8, 126.2, 122.0, 120.1, 117.8, 110.8, 102.0, 60.1, 59.6, 30.9, 13.4, 11.7; IR (KBr) ν (in cm^{-1}) 3461 (N−H stretching), 2098 (sp^2 C−H stretching), 2934 (sp^3 C−H stretching), 1631, 1563 (C═N stretching), 1512, 1467 (C═C stretching), 1408, 1381, 1307, 1263, 1097 (S═O stretching), 1062, 1003 (C−O stretching), 889, 824, 771, 726, 684, 609, 580; HR-MS (ESI) m/z calcd for $C_{21}H_{22}N_4O_2S$, 394.1463; found, 395.1535 $(M + H)^+$; HPLC >98%.

*1-Methyl-2-(((3-methyl-4-(2,2,2-trifluoroethoxy)pyridin-2-yl)methyl)sulfinyl)-5-(1H-pyrrol-1-yl)-1H-benzo[d]imidazole (**11o**) (23 mg, 15%).* ^{1}H NMR (400 MHz, $CDCl_3$) δ 8.09 (s, 1H), 7.80 (d, J = 1.7 Hz, 1H), 7.48−7.41 (m, 2H), 7.11 (t, J = 2.2 Hz, 2H), 6.37 (t, J = 2.2 Hz, 2H), 5.03−4.88 (m, 2H), 4.00 (s, 3H), 3.70 (s, 3H), 2.29 (s, 3H), 2.21 (s, 3H); ^{13}C NMR (100 MHz, $CDCl_3$) δ 164.4, 153.9, 149.7, 149.5, 142.8, 137.4, 134.7, 126.8, 126.2, 120.1, 119.0, 112.9, 110.6, 110.5, 60.1, 59.5, 31.0, 13.4, 11.7; IR (KBr) ν (in cm^{-1}) 3467 (N−H stretching), 3105 (sp^2 C−H stretching), 2940 (sp^3 C−H stretching), 1626, 1570 (C═N stretching), 1507, 1472 (C═C stretching), 1413, 1370, 1303, 1257, 1101 (S═O stretching), 1068, 997 (C−O stretching), 892, 829, 776, 730, 681, 615, 576; HR-MS (ESI) m/z calcd for $C_{21}H_{22}N_4O_2S$, 394.1463; found, 417.1355 $(M + Na)^+$; HPLC >98%.

*2-(((4-(2-Fluoroethoxy)-3-methylpyridin-2-yl)methyl)-thio)-5-(1H-pyrrol-1-yl)-1H-benzoimidazole (**10l**) (285 mg, 75%).* ^{1}H NMR (400 MHz, $CDCl_3$) δ 13.15 (br s, 1H), 8.39 (d, J = 5.7 Hz, 1H), 7.60−7.48 (m, 2H), 7.24 (dd, J = 8.7, 2.1 Hz, 1H), 7.10 (t, J = 2.2 Hz, 2H), 6.77 (d, J = 5.7 Hz, 1H), 6.35 (t, J = 2.2 Hz, 2H), 4.90−4.85 (m, 1H), 4.79−4.72 (m, 1H), 4.40 (s, 2H), 4.36−4.31 (m, 1H), 4.29−4.25 (m, 1H), 2.32 (s, 3H); ^{13}C NMR (100 MHz, $CDCl_3$) δ 163.9, 157.0, 147.3, 136.2, 121.6, 120.3, 116.1, 109.9, 106.2, 82.4 (q, $^1J_{CF}$ = 172 Hz), 67.6 (q, $^2J_{CF}$ = 36.3 Hz), 34.8, 10.9.

*2-(((4-(2-Fluoroethoxy)-3-methylpyridin-2-yl)methyl)-sulfinyl)-5-(1H-pyrrol-1-yl)-1H-benzo[d]imidazole (**11p**) (124 mg, 45%).* ^{1}H NMR (400 MHz, $CDCl_3$) δ 12.43 (br s, 1H), 8.28 (d, J = 5.6 Hz, 1H), 7.75−7.43 (m, 2H), 7.37 (dd, J = 8.7, 2.2 Hz, 1H), 7.09 (t, J = 2.0 Hz, 2H), 6.65 (d, J = 5.6 Hz, 1H), 6.37 (t, J = 2.0 Hz, 2H), 4.86−4.76 (m, 2H), 4.76 (t, J = 4.2 Hz, 1H), 4.68 (t, J = 4.2 Hz, 1H) 4.17 (ddddd, J = 23.0, 15.6, 11.5, 7.8, 4.1 Hz, 2H), 2.19 (s, 3H); ^{13}C NMR (100 MHz, $CDCl_3$) δ 163.3, 149.6, 148.4, 123.3, 120.1, 110.5, 106.3, 81.4 (d, $^1J_{CF}$ = 172 Hz), 67.4 (d, $^2J_{CF}$ = 20 Hz), 60.8, 11.2; IR (KBr) ν (in cm^{-1}) 3343 (N−H stretching), 3055 (sp^2 C−H stretching), 2965 (sp^3 C−H stretching), 1638, 1580 (C═N stretching), 1514, 1483 (C═C stretching), 1444, 1306, 1267, 1159, 1103 (S═O stretching), 993, 953 (C−O stretching), 897, 851, 798, 718, 637, 590, 565; HR-MS (ESI) m/z calcd for $C_{20}H_{19}FN_4O_2S$, 398.1213; found, 421.1104 $(M + Na)^+$; HPLC >98%.

*2-(((4-(2-Fluoroethoxy)-3-methylpyridin-2-yl)methyl)-sulfinyl)-1-methyl-5-(1H-pyrrol-1-yl)-1H-benzo[d]imidazole (**11q**) (33 mg, 17%).* ^{1}H NMR (400 MHz, $CDCl_3$) δ 8.18 (d, J = 5.6 Hz, 1H), 7.83 (d, J = 8.7 Hz, 1H), 7.41 (dd, J = 8.7, 2.1 Hz, 1H), 7.35 (d, J = 2.1 Hz, 1H), 7.13 (t, J = 2.2 Hz, 2H), 6.64 (d, J = 5.6 Hz, 1H), 6.38 (t, J = 2.2 Hz, 2H), 5.05−4.92 (m, 2H), 4.83 (t, J = 4.1 Hz, 1H), 4.71 (t, J = 4.1 Hz, 1H), 4.28−4.26 (m, 1H), 4.21−4.19 (m, 1H), 4.01 (s, 3H), 2.29 (s, 3H); ^{13}C NMR (100 MHz, $CDCl_3$) δ 163.1, 153.3, 150.7, 148.2, 140.3, 138.3, 137.1, 123.0, 122.0, 120.1, 117.7, 110.8, 106.0, 102.0, 81.5 (d, $^1J_{CF}$ = 172 Hz), 67.4 (d, $^2J_{CF}$ = 20 Hz), 59.5, 30.9, 11.2; IR (KBr) ν (in cm^{-1}) 3461 (N−H stretching), 3107 (sp^2 C−H stretching), 2944 (sp^3 C−H stretching), 1630, 1567 (C═N stretching), 1502, 1466 (C═C stretching), 1374, 1298, 1243, 1106 (S═O stretching), 1065, 989 (C−O stretching), 896, 825, 781, 724, 679, 613, 580; HR-MS (ESI) m/z calcd for $C_{21}H_{21}FN_4O_2S$, 412.1369; found, 435.1261 $(M + Na)^+$; HPLC >98%.

*2-(((4-(2-Fluoroethoxy)-3-methylpyridin-2-yl)methyl)-sulfinyl)-1-methyl-5-(1H-pyrrol-1-yl)-1H-benzo[d]imidazole (**11r**) (24 mg, 14%).* ^{1}H NMR (400 MHz, $CDCl_3$) δ 8.17 (d, J = 5.6 Hz, 1H), 7.80 (d, J = 2.0 Hz, 1H), 7.48−7.42 (m, 2H), 7.11 (t, J = 2.2 Hz, 2H), 6.64 (d, J = 5.6 Hz, 1H), 6.37 (t, J = 2.3 Hz, 2H), 5.06−4.92 (m, 2H), 4.83 (t, J = 4.1 Hz, 1H), 4.71 (t, J = 4.1 Hz, 1H), 4.28−4.25 (m, 1H), 4.21−4.19 (m, 1H), 4.02 (s, 3H), 2.29 (s, 3H); ^{13}C NMR (100 MHz, $CDCl_3$) δ 163.1, 153.8, 150.7, 148.2, 142.8, 137.4, 134.8, 123.0, 120.1, 119.0, 112.9, 110.6, 110.4, 106.0, 81.4 (d, $^1J_{CF}$ = 172 Hz), 67.4 (d, $^2J_{CF}$ = 20 Hz), 59.5, 31.0, 11.2; IR (KBr) ν (in cm^{-1}) 3471 (N−H stretching), 3113 (sp^2 C−H stretching), 2951 (sp^3 C−H stretching), 1621, 1572 (C═N stretching), 1499, 1468 (C═C stretching), 1381, 1307, 1259, 1161, 1106 (S═O stretching), 1055, 968 (C−O stretching), 879, 822, 778, 719, 657, 611, 568; HR-MS (ESI) m/z calcd for $C_{21}H_{21}FN_4O_2S$, 412.1369; found, 435.1261 $(M + Na)^+$; HPLC >98%.

*2-(((4-(2-Fluoroethoxy)-3-methylpyridin-2-yl)methyl)-sulfinyl)-1H-benzoimidazole (**11s**) (30 mg, 37%).* ^{1}H NMR (400 MHz, $CDCl_3$) δ 11.96 (br s, 1H), 8.31 (d, J = 5.7 Hz, 1H), 7.90−7.38 (m, 2H), 7.35−7.27 (m, 2H), 6.69 (d, J = 5.7 Hz, 1H), 4.87−4.70 (m, 2H), 4.82−4.78 (m, 1H), 4.71−4.67 (m, 1H), 4.28−4.23 (m, 1H), 4.20−4.16 (m, 1H), 2.19 (s,

DOI: 10.1021/acsomega.8b00975
ACS Omega 2018, 3, 7567−7579

3H); ^{13}C NMR (101 MHz, $CDCl_3$) δ 163.2, 153.4, 149.9, 148.4, 123.3, 106.2, 82.4 (d, $^1J_{CF}$ = 173.6 Hz), 77.5, 77.3, 77.1, 76.8, 67.4 (d, $^2J_{CF}$ = 20.4 Hz), 60.9, 11.2; IR (KBr) ν (in cm^{-1}) 3323 (N−H stretching), 3057 (sp^2 C−H stretching), 2951 (sp^3 C−H stretching), 1754, 1586 (C═N stretching), 1444, 1354 (C═C stretching), 1279, 1243, 1174, 1103 (S═O stretching), 978 (C−O stretching), 901, 858, 799, 743, 675, 582, 541; HR-MS (ESI) m/z calcd for $C_{16}H_{16}FN_3O_2S$, 333.0947; found, 356.0989 $(M + Na)^+$; HPLC >98%.

*2-(((4-(2-Fluoroethoxy)-3-methylpyridin-2-yl)methyl)-sulfinyl)-1-methyl-1H-benzoimidazole (**11t**) (28 mg, 33%).* 1H NMR (400 MHz, $CDCl_3$) δ 8.19 (d, J = 5.6 Hz, 1H), 7.82 (dt, J = 7.9, 1.0 Hz, 1H), 7.44−7.38 (m, 2H), 7.38−7.30 (m, 1H), 6.64 (d, J = 5.6 Hz, 1H), 5.04−4.92 (m, 2H), 4.85−4.80 (m, 1H), 4.73−4.68 (m, 1H), 4.29−4.23 (m, 1H), 4.22−4.17 (m, 1H), 4.02 (s, 3H), 2.28 (s, 3H); ^{13}C NMR (101 MHz, $CDCl_3$) δ 163.1, 152.5, 150.8, 148.2, 142.3, 136.6, 124.7, 123.4, 123.0, 121.2, 109.9, 106.0, 81.4 (d, $^1J_{C-F}$ = 173.1 Hz), 67.4 (d, $^2J_{C-CF}$ = 20.6 Hz), 59.5, 30.8, 11.2; IR (KBr) ν (in cm^{-1}) 3043 (sp^2 C−H stretching), 2947 (sp^3 C−H stretching), 1738, 1577 (C═N stretching), 1432, 1347 (C═C stretching), 1288, 1233, 1168, 1109 (S═O stretching), 985 (C−O stretching), 893, 851, 788, 731, 680, 577, 544; HR-MS (ESI) m/z calcd for $C_{17}H_{18}FN_3O_2S$, 347.1104; found, 370.1196 $(M + Na)^+$; HPLC >98%.

*2-(((6-Fluoro-4-methoxy-3,5-dimethylpyridin-2-yl)-methyl)sulfinyl)-1-methyl-1H-benzoimidazole (**11u**) (219 mg, 86%).* ^{1}H NMR ($CDCl_3$, 500 MHz) δ 7.81 (d, 1H, J = 8.1 Hz), 7.45−7.37 (m, 2H), 7.34 (ddd, J = 8.2, 6.7, 1.7 Hz, 1H), 4.88 (s, 2H), 4.04 (s, 3H), 3.71 (s, 3H), 2.25 (bs, 3H), 2.13 (bs, 3H); ^{13}C NMR ($CDCl_3$, 126 MHz) δ 167.4 (d, J = 7.9 Hz), 160.6 (d, J = 236.1 Hz), 152.0, 145.1 (d, J = 16.5 Hz), 142.0, 136.3, 125.1 (d, J = 5.4 Hz), 124.5, 123.2, 120.9, 112.1, (d, J = 32.5 Hz), 109.85, 60.2, 58.6, 30.6, 11.4, 8.26; ^{19}F NMR ($CDCl_3$, 470 MHz) δ −73.13 (s); HR-MS (ESI+) m/z calcd for $C_{17}H_{18}FN_3O_2S$, 347.1104; found, 348.1096 $(M + H)^+$; HPLC >98%.

*2-(((6-Fluoro-3,4-dimethoxypyridin-2-yl)methyl)sulfinyl)-1-methyl-1H-benzo[d]imidazole (**11v**) (429 mg, 91%).* ^{1}H NMR ($CDCl_3$, 500 MHz) δ 7.83−7.90 (m, 1H), 7.46−7.37 (m, 2H), 7.34 (ddd, J = 8.4, 6.9, 1.6 Hz, 1H), 6.35 (d, J = 1.3 Hz, 1H), 4.95 (d, J = 13 Hz, 1H), 4.76 (d, J = 13.0 Hz, 1H), 4.09 (s, 3H), 3.91 (s, 3H), 3.88 (s, 3H); ^{13}C NMR ($CDCl_3$, 126 MHz) δ 162.4 (d, J = 11.8 Hz), 159.0 (d, J = 235.3 Hz), 151.4, 143.7 (d, J = 4.9 Hz), 142.0, 140.8 (d, J = 17.6 Hz), 136.6, 124.5, 123.25, 120.9, 109.8, 93.1 (d, J = 44.9 Hz), 61.7, 56.2, 55.9, 30.7; ^{19}F NMR ($CDCl_3$, 470 MHz) δ −67.87 (s); HR-MS (ESI+) m/z calcd for $C_{16}H_{16}FN_3O_3S$, 349.0896; found, 350.0912 $(M + H)^+$; HPLC >98%.

■ ASSOCIATED CONTENT

Supporting Information

The Supporting Information is available free of charge on the ACS Publications website at DOI: 10.1021/acsomega.8b00975.

Experimental procedures and results and analytical data (PDF)

■ AUTHOR INFORMATION

Corresponding Author

*E-mail: patrick.riss@kjemi.uio.no.

ORCID

Patrick J. Riss: 0000-0002-3887-7065

Notes

The authors declare no competing financial interest.

■ ACKNOWLEDGMENTS

This study was funded by the faculty of Mathematics and Natural Sciences (SFI-leader P.J.R.), University of Oslo, and the Department of Chemistry, University of Oslo (startup grant to P.J.R.), the Norwegian Research Council (grant no. ES231553 awarded to P.J.R.), NMS AS (research support to P.J.R.), CORFO Innova Chile (grant no. 14IEAT-28666 awarded to H.A.), and PositronPharma SA. W.R. would like to thank the Kjemisk Institutt, UiO for a Ph.D. fellowship. We are grateful to Federico Carrión and Otto Pritsch, Institute Pasteur of Montevideo, for performing dynamic light scattering assays.

■ REFERENCES

(1) Alzheimer's Association. Alzheimer's disease facts and figures. *Alzheimer's Dementia* **2013**, *9*, 208−245.

(2) Feldman, H. H.; Woodward, M. The staging and assessment of moderate to severe Alzheimer disease. *Neurology* **2005**, *65*, S10−S17.

(3) Bossy-Wetzel, E.; Schwarzenbacher, R.; Lipton, S. A. Molecular pathways to neurodegeneration. *Nat. Med.* **2004**, *10*, S2−S9.

(4) Braak, H.; Braak, E. Neuropathological staging of Alzheimer-related changes. *Acta Neuropathol.* **1991**, *82*, 239−249.

(5) Lee, V. M.; Goedert, M.; Trojanowski, J. Q. Neurodegenerative tauopathies. *Annu. Rev Neurosci.* **2001**, *24*, 1121−1159.

(6) Komori, T. Tau-positive dial Inclusions in Progressive Supranuclear Palsy, Corticobasal Degeneration and Pick's Disease. *Brain Pathol.* **1999**, *9*, 663−679.

(7) Delacourte, A. Tauopathies: recent insights into old diseases. *Folia Neuropathol.* **2005**, *43*, 244−257.

(8) Ross, C. A.; Poirier, M. A. Protein aggregation and neuro-degenerative disease. *Nat. Med.* **2004**, *10*, S10−S17.

(9) Cedazo-Minguez, A.; Winblad, B. Biomarkers for Alzheimer's disease and other forms of dementia: clinical needs, limitations and future aspects. *Exp. Gerontol.* **2010**, *45*, 5−14.

(10) Guzmán-Martínez, L.; Farías, G. A.; Maccioni, R. B. Emerging non-invasive biomarkers for early detection of Alzheimer's disease. *Arch. Med. Res.* **2012**, *43*, 663−666.

(11) Mathis, C. A.; Klunk, W. E. Imaging tau deposits in vivo: progress in viewing more of the proteopathy picture. *Neuron* **2013**, *79*, 1035−1037.

(12) Small, G. W.; et al. In vivo brain imaging of tangle burden in humans. *J. Mol. Neurosci.* **2002**, *19*, 321−328.

(13) Villemagne, V. L.; et al. The challenges of tau imaging. *Future Neurol.* **2012**, *7*, 409−421.

(14) Villemagne, V. L.; Okamura, N. In vivo tau imaging: obstacles and progress. *Alzheimers Dementia* **2014**, *10*, S254−S264.

(15) Vermeiren, C.; et al. T807, a reported selective tau tracer, binds with nanomolar affinity to monoamine oxidase-A. *Alzheimer's Dementia* **2015**, *11*, P283.

(16) Goedert, M.; Spillantini, M. G. Pathogenesis of the tauopathies. *J. Mol. Neurosci.* **2011**, *45*, 425−431.

(17) Schafer, K. N.; Kim, S.; Matzavinos, A.; Kuret, J. Selectivity requirements for diagnostic imaging of neurofibrillary lesions in Alzheimer's disease: A simulation study. *Neuroimage* **2012**, *60*, 1724−1733.

(18) Hardy, J.; Allsop, D. Amyloid deposition as the central event in the aetiology of Alzheimer's disease. *Trends Pharmacol. Sci.* **1991**, *12*, 383−388.

(19) Pike, K. E.; et al. β-amyloid imaging and memory in non-demented individuals: evidence for preclinical Alzheimer's disease. *Brain* **2007**, *130*, 2837−2844.

DOI: 10.1021/acsomega.8b00975
ACS Omega 2018, 3, 7567−7579

(20) Okamura, N.; et al. Quinoline and benzimidazole derivatives: candidate probes for in vivo imaging of tau pathology in Alzheimer's disease. *J. Neurosci.* **2005**, *25*, 10857−10862.
(21) (a) Riss, P. J.; Aigbirhio, F. I. A simple, rapid procedure for nucleophilic radiosynthesis of aliphatic [^{18}F]trifluoromethyl groups. *Chem. Commun.* **2011**, *47*, 11873−11875. (b) Riss, P. J.; Ferrari, V.; Brichard, L.; Burke, P.; Smith, R.; Aigbirhio, F. I. Direct, nucleophilic radiosynthesis of [^{18}F]trifluoroalkyl tosylates: improved labelling procedures. *Org. Biomol. Chem.* **2012**, *10*, 6980−6986.
(22) Rojo, L. E.; Alzate-Morales, J.; Saavedra, I. N.; Davies, P.; Maccioni, R. B. Selective interaction of lansoprazole and astemizole with tau polymers: potential new clinical use in diagnosis of Alzheimer's disease. *J. Alzheimers Dis.* **2010**, *19*, 573−589.
(23) Riss, P. J.; et al. Radiosynthesis and characterization of astemizole derivatives as lead compounds toward PET imaging of τ-pathology. *MedChemComm* **2013**, *4*, 852−855.
(24) Fawaz, M. V.; et al. High affinity radiopharmaceuticals based upon lansoprazole for PET imaging of aggregated tau in Alzheimer's disease and progressive supranuclear palsy: synthesis, preclinical evaluation, and lead selection. *ACS Chem. Neurosci.* **2014**, *5*, 718−730.
(25) Shao, X.; et al. Evaluation of [^{11}C]N-methyl lansoprazole as a radiopharmaceutical for PET imaging of tau neurofibrillary tangles. *ACS Med. Chem. Lett.* **2012**, *3*, 936−941.
(26) Hitchcock, S. A.; Pennington, L. D. Structure−brain exposure relationships. *J. Med. Chem.* **2006**, *49*, 7559−7583.
(27) Ertl, P.; Rohde, B.; Selzer, P. Fast calculation of molecular polar surface area as a sum of fragment-based contributions and its application to the prediction of drug transport properties. *J. Med. Chem.* **2000**, *43*, 3714−3717.
(28) Meisenheimer, J. Ueber reactionen aromatischer nitrokörper. *Justus Liebigs Ann. Chem.* **1902**, *323*, 205−246.
(29) Waser, M.; et al. Development of a Scalable and Safe Process for the Production of 4-Chloro-2,3-dimethylpyridine-N-oxide as a Key Intermediate in the Syntheses of Proton Pump Inhibitors. *Org. Process Res. Dev.* **2010**, *14*, 562−567.
(30) Koenig, T. W.; Wieczorek, J. S. Reactions of trichloroacetyl chloride with 2-picoline N-oxide and pyridylcarbinols. *J. Org. Chem.* **1968**, *33*, 1530−1532.
(31) Ichihara, Y.; et al. Rational design and synthesis of 4-substituted 2-pyridin-2-ylamides with inhibitory effects on SH2 domain-containing inositol 5-phosphatase 2 (SHIP2). *Eur. J. Med. Chem.* **2013**, *62*, 649−660.
(32) Rédl, S.; Klecén, O.; Havlíček, J. Synthetic studies connected with the preparation of h+/k+-ATPase inhibitors rabeprazole and lansoprazole. *J. Heterocycl. Chem.* **2006**, *43*, 1447−1453.
(33) Reddy, G. M.; et al. Identification and characterization of potential impurities of rabeprazole sodium. *J. Pharm. Biomed. Anal.* **2007**, *43*, 1262−1269.
(34) Fier, P. S.; Hartwig, J. F. Selective CH fluorination of pyridines and diazines inspired by a classic amination reaction. *Science* **2013**, *342*, 956−960.
(35) Schöll, M.; et al. PET imaging of tau deposition in the aging human brain. *Neuron* **2016**, *89*, 971−982.
(36) *OECD Guidelines for Testing of Chemicals, No.117*; OECD: Paris, 1992.

DOI: 10.1021/acsomega.8b00975
ACS Omega 2018, 3, 7567−7579